

# 1 **Background Heterogeneity and Other Uncertainties in** 2 **Estimating Urban Methane Flux: Results from the** 3 **Indianapolis Flux (INFLUX) Experiment**

4  
5 Nikolay V. Balashov<sup>1\*,2,3</sup>, Kenneth J. Davis<sup>1</sup>, Natasha L. Miles<sup>1</sup>, Thomas  
6 Lauvaux<sup>1,4</sup>, Scott J. Richardson<sup>1</sup>, Zachary R. Barkley<sup>1</sup>, Timothy A. Bonin<sup>5,6</sup>

7  
8 <sup>1</sup>The Pennsylvania State University, University Park, Pennsylvania, USA

9 <sup>2</sup>NASA Postdoctoral Program, Universities Space Research Association, 7178 Columbia Gateway Drive,  
10 Columbia, MD, 21046, USA

11 <sup>3</sup>NASA Global Modeling and Assimilation Office (GMAO), Goddard Space Flight Center, Greenbelt,  
12 MD, 20771, USA

13 <sup>4</sup>Laboratory of Climate Sciences and Environment, Gif-sur-Yvette, France

14 <sup>5</sup>Cooperative Institute for Research in Environmental Sciences, Boulder, Colorado, USA

15 <sup>6</sup>Chemical Sciences Division, National Oceanic and Atmospheric Administration, Boulder, Colorado,  
16 USA

17 \*Former affiliation

18 *Correspondence to:* Nikolay V. Balashov (nvb5011@psu.edu)

## 19 **Abstract**

20 As natural gas extraction and use continues to increase, the need to quantify emissions of  
21 methane (CH<sub>4</sub>), a powerful greenhouse gas, has grown. Large discrepancies in Indianapolis CH<sub>4</sub>  
22 emissions have been observed when comparing inventory, aircraft mass-balance, and tower  
23 inverse modeling estimates. Four years of continuous CH<sub>4</sub> mole fraction observations from a  
24 network of nine towers as a part of the Indianapolis Flux Experiment (INFLUX) are utilized to  
25 investigate four possible reasons for the abovementioned inconsistencies: (1) differences in  
26 definition of the city domain, (2) a highly temporally variable and spatially non-uniform CH<sub>4</sub>  
27 background, (3) temporal variability in CH<sub>4</sub> emissions, and (4) the presence of unknown CH<sub>4</sub>  
28 sources. Reducing the Indianapolis urban domain size to be consistent with the inventory  
29 domain size decreases the CH<sub>4</sub> emission estimation of the inverse modeling methodology by  
30 about 35% and thereby lessens the discrepancy by bringing total city flux within the error range  
31 of one of the two inventories. Nevertheless, the inverse modeling estimate still remains about

32 40% higher than inventory estimates. Hourly urban background CH<sub>4</sub> mole fractions are shown  
33 to be spatially heterogeneous and temporally variable. Variability in background mole fractions  
34 observed at any given moment and a single location could be up to about 50 ppb depending on a  
35 wind direction, but decreases substantially when averaged over multiple days. Statistically  
36 significant, long-term biases in background mole fractions of 2-5 ppb are found from single point  
37 observations for most wind directions. Boundary layer budget estimates suggest that  
38 Indianapolis CH<sub>4</sub> emissions did not change significantly when comparing 2014 to 2016.  
39 However, it appears that CH<sub>4</sub> emissions may follow a diurnal cycle with daytime emissions (12-  
40 16 LST) approximately twice as large as nighttime emissions (20-5 LST). We found no  
41 evidence for significant CH<sub>4</sub> point sources that are otherwise missing from the inventories. The  
42 data from the towers suggest that the strongest CH<sub>4</sub> source in Indianapolis is South Side Landfill.  
43 Leaks from the natural gas distribution system that were detected with the tower network  
44 appeared localized and non-permanent and do not appear to constitute as large of a source of  
45 CH<sub>4</sub> as previously hypothesized by some top-down studies. Long-term averaging, spatially-  
46 extensive upwind mole fraction observations, mesoscale atmospheric modeling of the regional  
47 emissions environment, and careful treatment of the times of day and real representation of  
48 emission estimates are recommended for precise and accurate quantification of urban CH<sub>4</sub>  
49 emissions.

50

## 51 **1 Introduction**

52 From the beginning of the Industrial Revolution to 2011, atmospheric methane (CH<sub>4</sub>) mole  
53 fractions increased by a factor of 2.5 due to anthropogenic processes such as fossil fuel  
54 production, waste management, and agricultural activities (Ciais et al., 2013). The increase in

55 CH<sub>4</sub> is a concern as it is a potent greenhouse gas (GHG) with a global warming potential 28-34  
56 times greater than that of CO<sub>2</sub> over a period of 100 years (Myhre et al., 2013). The magnitudes  
57 of component CH<sub>4</sub> sources, and the causes of variability in the global CH<sub>4</sub> budget are not well  
58 understood although there is some evidence that biogenic emissions may play an important role  
59 in the recent CH<sub>4</sub> increases (Nisbet et al., 2016; Saunio et al., 2016). Improved understanding  
60 of CH<sub>4</sub> emissions is needed (National Academies of Sciences and Medicine, 2018).

61 In particular, the estimates of continental U.S. anthropogenic CH<sub>4</sub> emissions disagree.  
62 Inventories from Environment Protection Agency (EPA) and Emissions Database for Global  
63 Atmospheric Research (EDGAR) in 2008 reported emission values of 19.6 and 22.1 TgC y<sup>-1</sup>  
64 (U.S. EPA, 2013; European Commission Joint Research Centre and Netherlands Environmental  
65 Assessment Agency, 2010). However, top-down methodologies using aircraft and inverse  
66 modeling framework found emission values of 32.4 ± 4.5 TgC y<sup>-1</sup> for 2004 and 33.4 ± 1.4 TgC  
67 y<sup>-1</sup> for 2007-2008 respectively (Kort et al., 2008; Miller et al., 2013). Underestimation of natural  
68 gas (NG) production and agricultural sources are possible reasons for this disagreement (Miller  
69 et al., 2013; Brandt et al., 2014; Jeong et al., 2014). Efforts to reconcile GHGs emissions  
70 estimates using atmospheric methods and inventory assessment have sometimes succeeded  
71 (Schuh et al., 2013; Zavala-Araiza et al., 2015; Turnbull et al., 2019) when careful attention is  
72 given to the details of each method, and targeted atmospheric data are available. A recent  
73 synthesis of emissions from the U.S. NG supply chain demonstrated similar success and  
74 concluded that current inventory estimates of emissions from U.S. NG production are too low  
75 and that emission from NG distribution is one of the greatest remaining sources of uncertainty in  
76 the NG supply chain (Alvarez et al., 2018).

77           Due to the uncertainties in CH<sub>4</sub> emissions from NG distribution it is natural that urban  
78 emissions are of interest as well. For example, two studies (McKain et al., 2015; Hendrick et al.,  
79 2016) indicate that ~60-100% of Boston CH<sub>4</sub> emissions are attributable to the NG distribution  
80 system. Recent studies of urban CH<sub>4</sub> emissions in California indicate that the California Air  
81 Resources Board (CARB) inventory tends to underestimate the actual CH<sub>4</sub> urban fluxes possibly  
82 due to fugitive emissions from NG infrastructures in urban environments (Wunch et al., 2009;  
83 Jeong et al., 2016; Jeong et al., 2017). The accuracy and precision of atmospheric estimates of  
84 urban CH<sub>4</sub> emissions are limited by available atmospheric observations (Townsend-Small et al.,  
85 2012), potential source magnitude variability with time (Jackson et al., 2014; Lamb et al., 2016),  
86 errors in atmospheric transport modeling (Hendrick et al., 2016; Deng et al., 2017; Sarmiento et  
87 al., 2017), and complexity in atmospheric background conditions (Cambaliza et al., 2014; Karion  
88 et al., 2015; Heimbürger et al., 2017). In this work, detailed analysis of urban CH<sub>4</sub> mole  
89 fractions is performed for the city of Indianapolis to better understand the aforementioned  
90 uncertainties of urban CH<sub>4</sub> emissions.

91           The Indianapolis Flux Experiment (INFLUX; Davis et al., 2017) is a testbed for  
92 improving quantification of urban GHGs emissions and their variability in space and time.  
93 INFLUX (<http://influx.psu.edu>) is located in Indianapolis partly because of its isolation from  
94 other urban centers and the flat Midwestern terrain. It includes a very dense GHGs monitoring  
95 network, comprised of irregular insitu aircraft measurements (Heimbürger et al., 2017;  
96 Cambaliza et al., 2014), continuous in situ observations from communications towers using  
97 cavity ring-down spectroscopy (Richardson et al., 2017; Miles et al., 2017), and automated flask  
98 sampling systems for quantification of a wide variety of trace gases (Turnbull et al., 2015).  
99 Meteorological sensors include a Doppler lidar providing continuous boundary layer depth and



100 wind profiles, and tower-based eddy covariance measurements of the fluxes of momentum,  
101 sensible and latent heat (Sarmiento et al., 2017). The network is designed for emissions  
102 quantification using top-down methods such as tower-based inverse modeling (Lauvaux et al.,  
103 2016) and aircraft mass balance estimates (Cambaliza et al., 2015).

104 Lamb et al. (2016) compared Indianapolis CH<sub>4</sub> emissions estimates from a variety of  
105 approaches, specifically inventory, aircraft mass balances, and inverse modeling. The results  
106 revealed large mean differences among the city fluxes estimated from these methods (Fig. 1). In  
107 general, the inventory methods arrived at lower estimates of emissions compared to the  
108 atmospheric, or top-down approaches. CH<sub>4</sub> fluxes calculated using the aircraft mass balance  
109 technique varied considerably between flights, more than would be expected from propagation of  
110 errors of the component measurements (Cambaliza et al., 2014; Lamb et al., 2016). The  
111 atmospheric inverse estimate was significantly higher than the inventory and some of the  
112 aircraft-derived values.

113 Biogenic emissions from the city are dominated by a landfill close to downtown, and  
114 these emissions are thought to be fairly well known (GHG reporting program). Although  
115 evidence of possible variability in landfill emissions exists from Cambaliza et al. (2015), which  
116 used aircraft mass balance on five different occasions to calculate CH<sub>4</sub> flux from this landfill.  
117 Uncertainty in total city emissions is mainly driven by the uncertainty in thermogenic emissions,  
118 which are hypothesized to emerge largely from the NG distribution system (Mays et al., 2009;  
119 Cambaliza et al., 2015; Lamb et al., 2016). In this study, we explore potential explanations for  
120 the discrepancies in CH<sub>4</sub> emissions estimates from Indianapolis and posit methods and  
121 recommendations for the study of CH<sub>4</sub> emissions from other urban centers.

122 We examine four different potential explanations for the CH<sub>4</sub> flux discrepancies reported  
123 in Lamb et al. (2016): (1) inconsistent geographic boundaries between top-down and bottom-up  
124 studies, (2) heterogeneity in the urban scale CH<sub>4</sub> background and (3) temporal variability in  
125 urban emissions, both of which were not accounted for in top-down studies, and (4) CH<sub>4</sub> sources  
126 that are not accounted for in the inventories. Well-calibrated CH<sub>4</sub> sensors on the INFLUX tower  
127 network (Miles et al., 2017) collected continuous CH<sub>4</sub> observations from 2013 to 2016 and  
128 provide a unique opportunity to explore these issues.

129

## 130 **2 Methods**

131

### 132 **2.1 Experimental site**

133 This study uses data from a tower-based GHG observational network located in the city and  
134 surrounding suburbs of Indianapolis, Indiana in the Midwestern U.S. Prior studies have used  
135 varying definitions for the region of Indianapolis (Cambaliza et al., 2015, Lamb et al., 2016). In  
136 this work, we follow Gurney et al. (2012) and define Indianapolis as the area of Marion County.  
137 The flat terrain of the region simplifies interpretation of the atmospheric transport. The land-  
138 surface heterogeneity inherent in the urban environment (building roughness, spatial variations in  
139 the surface energy balance) does have a modest influence on the flow within the city and the  
140 boundary layer depth difference between the urban and rural areas (Sarmiento et al., 2017).

141 Figure 2 shows two domains that have been used for the evaluation of Indianapolis CH<sub>4</sub>  
142 emissions (Lamb et al., 2016; Lauvaux et al., 2016). The first domain is the whole area shown in  
143 the figure enclosing both Indianapolis and places that lie outside of its boundaries. This domain  
144 was used for the inversion performed in Lamb et al. (2016). The second domain is Marion

145 County outlined with a green dashed line. It is assumed here that this domain is much more  
146 representative of the actual Indianapolis municipal boundaries as this area encompasses the  
147 majority of the urban development associated with the city of Indianapolis (Gurney et al., 2012).  
148 The larger domain has three additional landfills that based on the EPA gridded inventory  
149 (Maasackers et al., 2016) increase Indianapolis CH<sub>4</sub> emissions by about 50% when compared to  
150 the smaller domain. The inversion explained in Lamb et al. (2016) has been rerun for two of the  
151 domains mentioned above and the results (Fig. 1) have been reexamined.

152

## 153 **2.2 INFLUX tower network**

154 The continuous GHG measurements from INFLUX are described in detail in Richardson et al.  
155 (2017). The measurements were made using wavelength-scanned cavity ring down  
156 spectrometers (CRDS, Picarro, Inc., models G2301, G2302, G2401, and G1301), installed at the  
157 base of existing communications towers, with sampling tubes secured as high as possible on each  
158 tower (39 – 136 m above ground level (AGL); Miles et al., 2017). A few towers also included  
159 measurements at 10 m AGL and one or two intermediate levels. While INFLUX tower in-situ  
160 measurements began in September 2010, here we focus on the CH<sub>4</sub> measurements from 2013 –  
161 2016. From June through December 2012, there were two or three towers with operational CH<sub>4</sub>  
162 measurements. By July 2013, five towers included measurements of CH<sub>4</sub>, and throughout the  
163 majority of the years 2015 – 2016 there were eight INFLUX towers with CH<sub>4</sub> measurements  
164 (Fig. 3). Flask to in-situ comparisons and round-robin style testing indicated compatibility  
165 across the tower network of 0.6 ppb CH<sub>4</sub> (Richardson et al., 2017). In this study we use hourly  
166 means of CH<sub>4</sub>.

167

### 168 **2.3 Meteorological data**

169 Wind data were measured at the Indianapolis International Airport (KIND), Eagle Creek Airpark  
170 (KEYE), and Shelbyville Municipal Airport (KGEZ). The data used are hourly values from the  
171 Integrated Surface Dataset (ISD) (<https://www.ncdc.noaa.gov/isd>) and 5-minute values directly  
172 from the Automated Surface Observing System (ASOS). A complete description of ASOS  
173 stations is available at <https://www.weather.gov/media/asos/aum-toc.pdf>. The accuracy of the  
174 wind speed measurements are  $\pm 1$  m/s or 5% (whichever is greater) and the accuracy of the wind  
175 direction is 5 degrees when the wind speed is  $\geq 2.6$  m/s. The anemometers are located at about  
176 10 meters AGL. The wind data reported in ISD are given for a single point in time recorded  
177 within the last 10 minutes of an hour and are closest to the value at the top of the hour.

178 The planetary boundary layer height (BLH) was determined from a Doppler lidar  
179 deployed in Lawrence, Indiana about 15 km to the northeast of downtown. The lidar is a Halo  
180 Streamline unit, which was upgraded to have extended range capabilities in January 2016. The  
181 lidar continuously performs a sequence of conical, vertical-slice, and staring scans to measure  
182 profiles of the mean wind, turbulence, and relative aerosol backscatter. All of these  
183 measurements are combined using a fuzzy-logic technique to automatically determine the BLH  
184 continuously every 20-min (Bonin et al., 2018). The BLH is primarily determined from the  
185 turbulence measurements, but the wind and aerosol profiles are also used to refine the BLH  
186 estimate. The BLHs are assigned quality-control flags that can be used to identify times when  
187 the determined BLH is unreliable, such as when the air is exceptionally clean, the BLH is below  
188 a minimum detectable height, or clouds and fog that attenuate the lidar signal exist. Additional  
189 details about the algorithm and the lidar operation for the INFLUX project are provided in Bonin

190 et al. (2018). Doppler lidar measurements are available at  
191 <https://www.esrl.noaa.gov/csd/projects/influx/>.

192

## 193 **2.4 Urban methane background**

194 Both aircraft mass balance and inverse modeling methodologies rely on an accurate estimation of  
195 the urban CH<sub>4</sub> enhancement relative to the urban CH<sub>4</sub> background in order to produce a reliable  
196 flux estimate (Cambaliza et al., 2014; Lamb et al., 2016). The CH<sub>4</sub> mole fraction enhancement is  
197 defined as,

$$C_{enhancement} = C_{downwind} - C_{bg} \quad (1)$$

198 where  $C_{downwind}$  is the CH<sub>4</sub> mole fraction measured downwind of a source and  $C_{bg}$  is the CH<sub>4</sub>  
199 background mole fraction, which can be measured upwind of the source, but this is not  
200 necessary. Background, as defined in this body of literature, is a mole fraction measurement that  
201 does not contain the influence of the source of interest, but which is assumed to accurately  
202 represent mole fractions that are upwind of the source of interest and measured simultaneously  
203 with the downwind mole fractions.

204 Aircraft mass balance studies of Indianapolis mentioned used two main methods to  
205 determine a background value. The first method calculates an average of the aircraft transect  
206 edges that lie outside of the city domain (Cambaliza et al., 2014). In the second approach, a  
207 horizontally varying background is introduced by linearly interpolating median background  
208 values of each of the transect edges (Heimbürger et al., 2017). In theory there is also a third  
209 method that uses an upwind transect as a background field, but in the studies above it was  
210 assumed that the edges are representative of an upwind flow. In the case of an inversion, it is  
211 common to pick a tower that is located generally away from urban sources and has on average

212 the smallest overall enhancement (Lavaux et al., 2016). Because choosing the background  
213 involves a degree of subjectivity (Heimbürger et al., 2017) we consider how these choices may  
214 influence emission estimates and introduce error, both random and systematic, using data from  
215 the INFLUX tower network.

216         Using tower network data from November 2014 through the end of 2016, two CH<sub>4</sub>  
217 background fields are generated for the city of Indianapolis based on two different sets of  
218 criteria. The notion is based on the fact that a choice of background is currently rather arbitrary  
219 in the literature (Heimbürger et al., 2017) and at every point in time it is possible to choose  
220 multiple background values that are equally acceptable for the flux estimation. In our case both  
221 approaches identify a tower suitable to serve as a background for each of the eight wind  
222 directions (N, NE, E, SE, S, SW, W, NW), where an arc of 45° represents a direction (e.g. winds  
223 from N are between 337.5° and 22.5°). Estimating background for different wind directions is  
224 implemented to more accurately represent upwind flow that is hopefully not contaminated by  
225 local sources.

226         Criterion 1 corresponds to a typical choice of a background in a case of tower inversion  
227 and is based on the concept that the lowest CH<sub>4</sub> mole fraction measured at any given time is not  
228 affected by the city sources and therefore is a viable approximation of the background CH<sub>4</sub> mole  
229 fractions outside of the city (Miles et al., 2017; Lavaux et al., 2016). Given this assumption, the  
230 tower with the lowest median of the CH<sub>4</sub> enhancement distribution (calculated by assuming the  
231 lowest measurement among all towers at a given hour as a background) for each of the wind  
232 directions over the November 2014 through December 2016 time period is chosen as a  
233 background site (Miles et al., 2017). Criterion 2 requires that the tower is outside of Marion  
234 County (outside of the city boundaries) and is not downwind of any known regional CH<sub>4</sub> source

235 (Fig. 2). For some wind directions, there are multiple towers that could qualify as a background;  
236 we pick towers in such a manner that they are different for each criterion given a wind direction  
237 in order to calculate the error associated with the use of different but acceptable backgrounds.  
238 The towers used for both criteria and for each of the eight wind directions are displayed in Table  
239 1. Quantifying differences between these two backgrounds allows for an opportunity to better  
240 understand the degree of uncertainty that exists in the atmospheric CH<sub>4</sub> background at  
241 Indianapolis.

242 To make the comparison as uniform as possible only data from 12-16 LST are utilized  
243 (all hours are inclusive) when the boundary layer is typically well-mixed (Bakwin et al., 1998).  
244 A lag 1 autocorrelation is found between 12-16 LST hours, i.e. the hourly afternoon data are  
245 correlated to the next hour, but the correlation is not significant for samples separated by two  
246 hours or more. Therefore, hours 13 and 15 LST are eliminated to satisfy the independence  
247 assumption for hourly samples. Furthermore, we make an assumption that the data satisfy steady  
248 state conditions. If the difference between consecutive hourly wind directions exceeds 30  
249 degrees or the difference between hours 16 and 12 LST exceeds 40 degrees, the day is  
250 eliminated. Days with average wind speeds below 2 m/s are also eliminated due to slow  
251 transport across the city (the transit time from tower 1 to tower 8 is about 7 hours at a wind speed  
252 of 2 m/s).

253

## 254 **2.5 Frequency and bivariate polar plots**

255 Frequency and bivariate polar plots are used in this work to gain more knowledge regarding CH<sub>4</sub>  
256 background variability based on criteria 1 and 2, and to identify sources located within the city.  
257 To generate these polar plots, we use the *openair* package (from R programming language)

258 created specifically for air quality data analysis (Carslaw and Ropkins, 2012). Bivariate and  
259 frequency polar plots indicate the variability of a pollutant concentration at a receptor (such as an  
260 observational tower) as a function of wind speed and wind direction, preferably measured at the  
261 location of the receptor or within several kilometers of the receptor. The frequency polar plot is  
262 generated by partitioning the CH<sub>4</sub> hourly data into the wind speed and direction bins of 1 m s<sup>-1</sup>  
263 and 10° respectively. To generate bivariate polar plots, wind components  $u$  and  $v$  are calculated  
264 for hourly CH<sub>4</sub> mole fraction values, which are fitted to a surface using a Generalized Additive  
265 Model (GAM) framework in the following way,

$$\sqrt{C} = \beta + s(u, v) + \epsilon \quad (2)$$

266 where  $C$  is the CH<sub>4</sub> mole fraction transformed by a square root to improve model diagnostics  
267 such as a distribution of residuals,  $\beta$  is mean of the response,  $s$  is the isotropic smoothing  
268 function of the wind components  $u$  and  $v$ , and  $\epsilon$  is the residual. For more details on the model  
269 see Carslaw and Beevers (2013).

270

## 271 **2.6 Temporal variability and approximate flux estimation**

272 Temporal variability may play an important role in the quantification of urban CH<sub>4</sub> emissions.  
273 Lamb et al. (2016) suggested that temporal variability might partially explain the differences  
274 among CH<sub>4</sub> flux estimates shown in Figure 1. If temporal variability of CH<sub>4</sub> emissions exists  
275 within the city, disagreements in the CH<sub>4</sub> flux between studies could be attributed to differences  
276 in their sampling period. Because the INFLUX tower data at Indianapolis contain measurements  
277 at all hours of the day over multiple years, we can utilize this dataset to better understand the  
278 temporal variability in methane emissions in the city.



279 We apply a simplified atmospheric boundary layer budget, not to estimate precisely the  
 280 actual city emissions, but rather to evaluate temporal variability of the emissions. We begin by  
 281 assuming CH<sub>4</sub> emissions  $Q_a$  (mass per unit time per unit area) are not chemically active and are  
 282 constant over a distance  $\Delta x$  spanning a significant portion of the city. The next assumption is  
 283 that a CH<sub>4</sub> plume measured downwind of the city is well mixed within a layer of depth  $H$  (which  
 284 is the same as BLH). We treat wind speed  $u$  as constant within the layer for every hour  
 285 considered. Given the above-mentioned assumptions we can write a continuity equation  
 286 describing mass conservation of CH<sub>4</sub> concentration  $C$  within a box in the following fashion,

$$\Delta x H \frac{\partial C}{\partial t} = \Delta x Q_a + uH(C_b - C) + \Delta x \frac{\partial H}{\partial t} (C_a - C) \quad (3)$$

287 where  $C_b$  is the CH<sub>4</sub> concentration upwind of the city (or background), and  $C_a$  is the CH<sub>4</sub>  
 288 concentration above the mixed layer (Hanna et al., 1982; Arya, 1999; Hiller et al., 2014). The  
 289 left hand side of the equation represents the change in CH<sub>4</sub> concentration with time,  $\Delta x Q_a$   
 290 denotes a constant CH<sub>4</sub> source over the distance  $\Delta x$ ,  $uH(C_b - C)$  indicates a change of CH<sub>4</sub>  
 291 concentration due to horizontal advection, and finally  $\Delta x \frac{\partial H}{\partial t} (C_a - C)$  term accounts for the  
 292 vertical advection and encroachment processes that result from changing BLH. By assuming  
 293 steady state conditions ( $\frac{\partial C}{\partial t} = 0$  and  $\frac{\partial H}{\partial t} = 0$ ), the equation can be simplified to

$$Q_a = \frac{uH(C - C_b)}{\Delta x} \quad (4)$$

294 We use equation 4 to estimate hourly CH<sub>4</sub> emissions ( $Q_a$ ) from Indianapolis (see  
 295 assumptions in the paragraph below) given hourly averaged data of  $H$  from the lidar positioned  
 296 in the city, wind speed ( $u$ ) from the local weather stations, and upwind ( $C_b$ ) and downwind ( $C$ )  
 297 CH<sub>4</sub> mole fractions measured (and then converted to concentrations) at towers 1, 8, and 13

298 (depending on a wind direction) using data from heights of 40 m, 41 m, and 87 m respectively  
299 (see Fig. 2).

300 The CH<sub>4</sub> concentrations are derived from CH<sub>4</sub> mole fractions by approximating average  
301 molar density of dry air (in mol m<sup>-3</sup>) within the boundary layer for every hour of the day, where  
302 variability of pressure with altitude is calculated using barometric formula and it is assumed that  
303 temperature decreases with altitude by 6.5 K per kilometer. The hourly surface data for pressure  
304 and temperature are taken from KIND weather station. The difference between concentrations  
305  $C - C_b$  is instantaneous and not lagged, where  $C_b$  represents air parcel entering the city and  $C$   
306 represents the same air parcel exiting the city (Turnbull et al., 2015). The CH<sub>4</sub> enhancements  
307  $C - C_b$  are estimated for daytime by averaging observations spanning 12-16 LST and for  
308 nighttime by averaging observations spanning 20-5 LST. These time periods are based on lidar  
309 estimations of when on average  $H$  varies the least. The day and night were required to contain at  
310 least 3 and 9 hourly CH<sub>4</sub> values respectively for averaging to occur, otherwise the day/night is  
311 eliminated. Observations when  $H$  is below 100 m are not used to avoid the cases when  
312 measurements from towers may be above the boundary layer. In order to better achieve the  
313 assumption that the boundary layer is fully mixed (especially at night), all hours with wind  
314 speeds below 4 m/s are eliminated (Van De Wiel., 2012). To approximate the emissions of the  
315 whole city we need to know the approximate area of the city and the distance over which the  
316 plume is affected by the city CH<sub>4</sub> sources. The area of the city is about 1024 km<sup>2</sup> (the area of  
317 Marion County) and the length that plume traverses when it is over the city ranges from 32 to 35  
318 km depending on which downwind tower is used. We assume that CH<sub>4</sub> measurements at towers  
319 8 and 13 are representative of a vertically well-mixed city plume as the towers are located  
320 outside of the city boundaries and allow for sufficient vertical mixing to occur. For S and SW

321 wind directions tower 8 observations are used to represent downwind conditions with  
322 background observations coming from towers 1 and 13, respectively (based on criterion 1 shown  
323 in Table 1). For W wind direction, tower 13 observations represent the downwind with  
324 background obtained from tower 1. The wind direction is required to be sustained for at least 2  
325 hours, otherwise the data point is eliminated.

326

## 327 **2.7 Indianapolis CH<sub>4</sub> sources**

328 Only a few known CH<sub>4</sub> point sources exist within Indianapolis (Cambaliza et al., 2015, Lamb et  
329 al., 2016). The Southside Landfill (SSLF), located near the center of the city, is thought to be the  
330 largest point source in the city with emissions ranging between about 28 mol/s (inventory from  
331 Maasakkers et al. (2016), GHG reporting program, and inverse estimates from ground-based  
332 mobile sampling employed in Lamb et al. (2016)) and 45 mol/s (aircraft; Cambaliza et al.  
333 (2015)) depending on an emission estimation methodology. However, using Cambaliza et al.  
334 (2015) aircraft data and applying a different background formulation Lamb et al. (2016) found  
335 emission values of SSLF closely agreeing with 28 mol/s estimate. SSLF could account for as  
336 little as 33% (top-down from Cambaliza et al., 2015) or as much as 63% (inventory from  
337 Maasakkers et al., 2016) of total Marion County CH<sub>4</sub> emissions. Other city point sources are  
338 comparatively small; the wastewater treatment facility located near SSLF contributes about 3-7  
339 mol/s (inventory from Lamb et al. 2016), and the transmission-distribution transfer station at  
340 Panhandle Eastern Pipeline (also known as a city gate and further in this study abbreviated as  
341 PEP) is estimated to be about 1 mol/s (inventory from Lamb et al. 2016). The remaining CH<sub>4</sub>  
342 sources, mainly from NG infrastructure leaks and livestock, are considered to be diffuse sources  
343 and are not well known. Potential sources of emissions related to NG activities include gas

344 regulation meters, transmission and storage, distribution leaks, and Compressed Natural Gas  
345 (CNG) fleets. These diffuse NG sources account for 21-67% (this value varies due to the  
346 uncertainty in SSLF emissions) of the city emissions or 20 mol/s (inventory from Maasakkers et  
347 al., 2016) to 64 mol/s (top down from Cambaliza et al., 2015). Livestock emissions for Marion  
348 County are estimated to be around 1.5 mol/s (inventory from Maasakkers et al., 2016). An  
349 important question remains of whether SSLF or NG is the dominant CH<sub>4</sub> source in Indianapolis,  
350 or whether they are approximately equal.

351

### 352 **3 Results and discussion**

353

#### 354 **3.1 Inversion and city boundaries**

355 A significant portion of CH<sub>4</sub> emissions across the U.S. can be characterized by numerous large  
356 point sources scattered throughout the country rather than by broad areas of smaller  
357 enhancements (Maasakkers et al., 2016). Because of this, the total emissions for a given domain  
358 can be very sensitive to how that domain is defined. A small increase or decrease in the domain  
359 area could add or remove a large point source and significantly impact the total emissions  
360 defined within the domain.

361 In the case of Indianapolis, this issue became apparent when the emissions were  
362 calculated using an atmospheric inversion model (Lamb et al., 2016; Lauvaux et al., 2016). The  
363 atmospheric inversion solved for fluxes in domain 1 (Fig. 2), which significantly increased the  
364 estimated emissions in comparison with the inventory values that were gathered mainly within  
365 Marion County (domain 2). When reduced to domain 2, inverse modeling emission estimates  
366 decrease to 107 mol/s, which falls within an error bar of Lamb et al. (2016) inventory estimate.  
367 This difference is significant and could at least partially explain the discrepancy shown in Figure  
368 1 between the emission values from the inventories and emission results from the inverse

369 modeling. However, even the decreased inverse modeling estimate is about 40% higher than the  
370 inventories.

371 Additionally, the subject of the domain is relevant for airborne mass balance flights  
372 because a priori the magnitude and variability of background plume is unknown and could be  
373 easily influenced by upwind sources. The issue of background is discussed further in the next  
374 section.

375

### 376 **3.2 Variability in CH<sub>4</sub> background**

377 Comparisons between criterion 1 and criterion 2 CH<sub>4</sub> background mole fractions as a  
378 function of wind speed and direction are visualized using frequency and bivariate polar plots  
379 (Fig. 4). Both backgrounds generally agree on the higher CH<sub>4</sub> originating from the SW, SE, and  
380 E wind directions (Figs. 4c-f); however, the values themselves differ especially when winds are  
381 from NW, SW, and SE. As background difference plots (Figs. 4g-h) indicate, there is a  
382 noticeable variability between the magnitudes of the CH<sub>4</sub> backgrounds, where criterion 2, by  
383 design, typically has higher background mole fractions. The background differences, at a given  
384 hour, suggest that the CH<sub>4</sub> field flowing into the city is heterogeneous with differences between  
385 towers ranging from 0 to over 45 ppb (Fig. 4g). Because large gradients in CH<sub>4</sub> background over  
386 the city could pose challenges for flux estimations using top down methods such as inverse  
387 modeling and aircraft mass balance, it is imperative to establish whether the background  
388 differences vary randomly or systematically and how to choose a background to minimize these  
389 errors.

390 To further understand the nature of background variability we calculate the mean,  
391 standard deviation, and standard error of background hourly differences between criterion 2 and

392 criterion 1 from November 2014 to December 2016 for each of the eight wind directions  
393 mentioned in Table 1. The results are shown in Figure 5. Systematic bias is evident for the SE,  
394 S, SW, W, and NW wind sectors, whereas random error dominates N, NE, and E wind  
395 directions. Wind directions showing statistically significant bias have mean biases ranging from  
396 2 to 5 ppb, with values as large as 8 ppb falling within the range of  $2 \times$  standard error. Standard  
397 deviation plot indicates potential background discrepancy that can occur on any given day, where  
398 W wind direction is the least variable with  $2 \times$  standard deviation close to 20 ppb, while SE wind  
399 direction is the most variable with  $2 \times$  standard deviation falling at about 50 ppb.

400 Random errors in the mole fractions of background differences (biases) are also  
401 important and are a function of the length of the data record. We quantify the random error in  
402 the CH<sub>4</sub> background mole fraction differences using the bootstrap method by randomly sampling  
403 2 to 150 hours (small and large sample size) of the background CH<sub>4</sub> differences for each of the  
404 wind directions with replacement (we make the assumption that our differences are independent  
405 since we eliminated lag 1 autocorrelation from the data). This sub-sampling experiment is  
406 repeated 5000 times (Efron and Tibshirani, 1986). The standard deviations of the mean  
407 (standard error) of the 5000 simulated differences are calculated for each wind direction. The  
408 resulting standard errors of the city CH<sub>4</sub> background differences, multiplied by 2 to represent the  
409 95% confidence intervals, are shown as a function of the length of the data record in Figure 6.  
410 Because random error falls as sample size grows it makes sense to assign a threshold indicating a  
411 minimum number of samples needed to achieve a theoretical precision for each wind direction.

412 One way to assign a required precision would be to make sure that the standard error  
413 (random error) reaches a point where it is less than Indianapolis enhancement of about 12 ppb (a  
414 higher estimate of the Indianapolis enhancement from section 3.3) by a factor of 2 when

415 combined with a bias (Table 2). Meaning that the sum of bias and standard error must be at most  
416 6 ppb. In this approach each wind direction would have a different threshold because of the  
417 differences in biases. For instance, given this requirement NW direction would need a random  
418 error of 1 since its bias is 5. For NW direction, this threshold would require more than 150  
419 samples. For N direction on the other hand, where the bias is 1, the requirement is fulfilled when  
420 random error crosses 5 ppb at 74 samples. Now we consider these random and systematic errors  
421 in CH<sub>4</sub> background differences in the context of Indianapolis urban CH<sub>4</sub> emissions.

422 For Indianapolis, using INFLUX tower network, we estimated that depending on sample  
423 size (number of hours sampled) and wind direction, background gradient across the city over 12-  
424 16 LST could vary from 0 to about 50 ppb (Fig. 5b). Given that the average afternoon CH<sub>4</sub>  
425 enhancement of the city is around 8-12 ppb (section 3.3; Fig. 7; Cambaliza et al., 2015; Miles et  
426 al., 2017), the error on the estimated emissions could easily be over 100% if the analysis does not  
427 approach the issue of background with enough sampling. A sample size of about 50 independent  
428 hours significantly decreases background uncertainty for N, NE, E, S, and W wind directions and  
429 allows for a more accurate assessment of the CH<sub>4</sub> emissions at Indianapolis. For CH<sub>4</sub> sources  
430 with a significantly larger signal than their regional background, the mentioned background  
431 variability becomes less impactful on results, but because Indianapolis is a relatively small  
432 emitter of CH<sub>4</sub>, and because there are relatively large sources outside of the city, uncertainties  
433 due to background estimation are comparatively large. Our uncertainty assessment suggests that  
434 the highly variable CH<sub>4</sub> emission values of Indianapolis from aircraft mass balance calculations  
435 shown in Figure 1 are at least partially due to the variability in the urban CH<sub>4</sub> background of  
436 Indianapolis.

437

### 438 3.3. Temporal variability of methane enhancements and fluxes in Indianapolis

439 Figure 7 presents average CH<sub>4</sub> mole fraction enhancements and flux calculations  
440 (equation 4) at towers 8 and 13 for years 2014, 2016, and 2013-2016 (for the detailed  
441 methodology see section 2.6). The years of 2014 and 2016 are chosen for temporal comparison  
442 because they do not contain major BLH data gaps. The error bars in the figure show the standard  
443 error multiplied by 2 indicating 95% confidence interval of each average.

444 One of the more interesting features in the Figure 7 is a day/night variability of CH<sub>4</sub>  
445 emissions at Indianapolis. The most prominent example of this feature is found in Figure 7c,  
446 where the estimates for both years suggest that daytime emissions are approximately twice as  
447 large as the emissions at night. The decrease of the CH<sub>4</sub> emissions at night also appears in tower  
448 13, but the errors are too high in those estimates to make any definitive conclusions. A similar  
449 urban CH<sub>4</sub> emissions diurnal variability is reported by Helfter et al. (2016) in their study of  
450 GHGs for London, UK, where they attribute diurnal variation of CH<sub>4</sub> emissions to the NG  
451 distribution network activities, fugitive emissions from NG appliances, and to temperature-  
452 sensitive CH<sub>4</sub> emission sources of biogenic origin (such as a landfill). Taylor et al. (2018)  
453 suggest that CH<sub>4</sub> emissions from landfills exhibit a diurnal cycle with higher emissions in early  
454 afternoon and 30-40% lower emissions at night.

455 With regard to yearly temporal variability we are only able to compare years 2014 and  
456 2016 due to limited BLH data for other years. Results from both towers suggest that  
457 Indianapolis overall CH<sub>4</sub> emissions did not change significantly between 2014 and 2016.  
458 Although it is important to be cautious about interpreting actual flux estimations given the  
459 assumptions mentioned in section 2.6, it is interesting to note that the flux values from both  
460 towers average at about 70 mol/s, which puts our value right in between inventory and inversion



461 estimates shown in Figure 1. If we assume that SSLF emissions are generally known (GHG  
462 reporting program) that would indicate that emissions from NG distribution are likely to be  
463 somewhat higher than both of the inventories currently estimate and consistent with the larger  
464 error bar of Lamb et al. (2016) inventory calculation. Another possible scenario is that SSLF  
465 emissions are higher than what is currently assumed. Given these complexities, uncertainty  
466 regarding the exact emissions from NG distribution at Indianapolis still remains.

467

### 468 **3.4 Methane Sources in Indianapolis**

469 Bottom-up emission inventories have difficulty tracking changes in sources over time. Our  
470 continuous tower network observations can monitor temporal and spatial variability in sources of  
471 CH<sub>4</sub> in Indianapolis. To do so we employ the aforementioned bivariate polar plots to verify  
472 known sources and potentially identify unknown sources across the city. We compare two time  
473 periods, 2014-2015 (two full years) and 2016. Figure 8 displays bivariate polar plots of CH<sub>4</sub>  
474 enhancements using criterion 1 background at 9 INFLUX towers in Indianapolis over the two  
475 years of 2014 and 2015. Figure 9 shows the same plot, but for the year 2016. Here we have  
476 separated 2016 from 2014-2015 because of different results noted during these times.

477         The images reveal that the most consistent and strongest source in the city is the SSLF.  
478 This is most evident from the 40+ ppb CH<sub>4</sub> enhancements detected at towers 7, 10 and 11  
479 coming from the location of the SSLF (by triangulation). Enhancements from the landfill appear  
480 to also be detectable at towers 2, 4, 5, and 13. Based on these observations it can be concluded  
481 that there are no other point sources in Marion County comparable in size to the SSLF. A small  
482 fraction of the SSLF plume is likely due to the co-located wastewater facility, but the inventory  
483 estimates suggest that the wastewater treatment facility is responsible for no more than 7% of

484 this plume (Cambaliza et al., 2015; Massakkers et al., 2016). The PEP, located in the  
485 northwestern section of the city, may be partially responsible for a plume of 5-10 ppb at towers 5  
486 and 11. However, the plume is less detectable using the criterion 2 background value that has  
487 higher background (using tower 8 as a background) from NW wind direction (not shown),  
488 adding uncertainty to the true magnitude of the enhancement from this source. The same is true  
489 for towers 2 and 13, which have pronounced plumes when winds are from the NW with the  
490 criterion 1 background, but when background 2 is used these plumes vanish (not shown). Such  
491 inconsistency makes it difficult to attribute these plumes to a specific source.

492 Another important point is the cluster of large enhancements surrounding tower 10 in  
493 2014-2015. Because no other tower sees these enhancements (at least at comparable  
494 magnitudes), we believe that these plumes are the result of local NG leaks likely from residential  
495 sector of Indianapolis. These plumes are not consistent temporally or spatially as they mostly  
496 disappear in 2016, potentially indicating that they are transient and localized NG distribution  
497 leaks. It is difficult to ascertain the exact combined magnitude of these leaks since they mix  
498 together with SSLF into an aggregated city plume when observed from downwind towers such as  
499 8 and 13. Yet, none of these leaks appear to be even remotely close in magnitude to the  
500 emissions that originate from SSLF. Thus, the diffuse NG source suspected to be twice as large  
501 as the SSLF source (Lamb et al., 2016) does not appear to be supported by these data. This  
502 assertion questions conclusions made by Cambaliza et al. (2015), who attributed most of the CH<sub>4</sub>  
503 emitted by Indianapolis to NG related activities. We hypothesize that the relatively high  
504 Indianapolis CH<sub>4</sub> emissions (see Fig. 1) reported by Cambaliza et al. (2015) are the result of the  
505 low sample size of airborne flux estimates making it prone to large random errors (see section  
506 3.2). However, our flux estimations at towers 8 and 13 discussed in the previous section do

507 imply that emissions from NG distribution may be higher than estimated by the inventories  
508 indicating that an overall NG contribution may be comparable in strength to SSLF. This  
509 discrepancy requires further investigation.

510

#### 511 **4 Conclusions**

512 We have examined four potential contributions to discrepancies between urban top-down and  
513 bottom-up estimates of CH<sub>4</sub> emissions from Indianapolis: domain definition, heterogeneous  
514 background mole fractions, temporal variability in emissions, and sources missing from  
515 inventories. Results indicate that the urban domain definition is crucial for the comparison of the  
516 emission estimates among various methods. Atmospheric inverse flux estimates for Marion  
517 County, which is similar to the domain that is analyzed by inventory and airborne mass balance  
518 methodologies (Mays et al., 2009, Cambaliza et al., 2014, Lamb et al., 2016), is 107 mol/s  
519 compared to 160 mol/s that is estimated for the larger domain (Hestia inventory domain; Gurney  
520 et al., 2012). This partially explains higher emissions in inverse modeling estimates shown by  
521 Lamb et al. (2016); however, 107 mol/s is still about 40-50% higher than what EPA and Lamb et  
522 al. (2016) find in their inventories (Fig. 1).

523 To better understand background variability at Indianapolis two different but acceptable  
524 background estimates, based on specific criteria for each wind direction, and their differences are  
525 used to assess heterogeneity of CH<sub>4</sub> background at Indianapolis. Background criterion 1 looks  
526 for a tower that is consistently lower than other towers, while background criterion 2 picks a  
527 tower that is outside of Marion County domain and is not downwind of any nearby sources as  
528 determined by EPA 2012 inventory. We focus on midday atmospheric conditions to avoid the  
529 complexities of vertical stratification in the stable boundary layer. The midday Indianapolis

530 atmospheric CH<sub>4</sub> mole fraction background is shown to be heterogeneous with 2-5 ppb  
531 statistically significant biases for NW, W, SW, S and SE wind directions. Random errors of  
532 background differences are a function of sample size and decrease as a number of independent  
533 samples increase. Small sample sizes, such as a few hours of data from a single point, are prone  
534 to random errors on the order of 10-30 ppb in the CH<sub>4</sub> background, similar to the magnitude of  
535 the total enhancement from the city of Indianapolis, which is estimated to be on average around  
536 10-12 ppb. Longer-term sampling and/or more extensive background sampling are necessary to  
537 reduce the random errors. Sample size required to reduce random errors of background  
538 differences to an acceptable value for flux calculation is largely dependent on a wind direction.  
539 Both bias (long-term average of background differences) and its random error are important  
540 when estimating total background uncertainty. The results indicate that N, NE, E, S, and W  
541 wind directions are more favorable for flux estimation and would require multiple days of  
542 measurements (e.g. about 50 independent hours of measurements) to reduce background  
543 uncertainty to about 6 ppb, which is half the magnitude of the typical CH<sub>4</sub> enhancement from  
544 Indianapolis. The remaining wind directions would require over 150 independent hourly  
545 measurements to achieve similar precision. We also estimate that depending on a wind direction  
546 for any given hour the spatial variability in background can be anywhere from 0 to 50 ppb. This  
547 uncertainty in the CH<sub>4</sub> background may partially explain Heimburger et al. (2017) finding of  
548 large variability in airborne estimates of Indianapolis CH<sub>4</sub> emissions. Given many samples, the  
549 airborne studies converge to an average value of CH<sub>4</sub> flux that is noticeably closer to the  
550 inventory estimates for Indianapolis than several of the individual estimates presented in Figure  
551 1.

552 Measurement and analysis strategies can minimize the impacts of these sources of error.  
553 Spatially extensive measurement of upwind CH<sub>4</sub> mole fractions are recommended. For towers or  
554 other point-based measurements, multiple upwind measurement locations are clearly beneficial.  
555 For the aircraft mass balance approach, we recommend an upwind transect to be measured,  
556 lagged in time if possible, to provide a more complete understanding of the urban background  
557 conditions. Complex background conditions might suggest that data from certain days or wind  
558 directions should not be used for flux calculation. Finally, a mesoscale atmospheric modeling  
559 system informed with the locations of important upwind CH<sub>4</sub> sources can serve as a powerful  
560 complement to the atmospheric data (Barkley et al., 2017). Such simulations can guide sampling  
561 strategies, and aid in interpretation of data collected with moderately complex background  
562 conditions.

563 With regard to temporal variability, no statistically detectable changes in the emission  
564 rates were observed when comparing 2014 and 2016 CH<sub>4</sub> emissions. However, a large  
565 difference between day and night CH<sub>4</sub> emissions was implied from a simple budget estimate.  
566 Night (20-5 LST) emissions may be 2 times lower than the emissions during the afternoon (12-  
567 16 LST) hours. Because prior estimates of top-down citywide emissions are derived using  
568 afternoon-only measurements, overall emissions of Indianapolis may be lower than these studies  
569 suggest. This bias may be present in studies performed in other cities as well. Our study  
570 suggests that day/night differences in CH<sub>4</sub> emissions must be understood if regional emission  
571 estimates are to be calculated correctly. Long-term, tower-based observations are an effective  
572 tool for understanding and quantifying multi-year variability in urban emissions.

573 One final point addressed in this study is the location of major CH<sub>4</sub> sources in  
574 Indianapolis. Analysis of the INFLUX observation data suggests that inventories for

575 Indianapolis are mostly accurate and that there is no clear evidence of a large, diffuse NG source  
576 of CH<sub>4</sub> as implied by Lamb et al. (2016). The only major source in the city is SSLF and it is  
577 observed at multiple towers. There is an evidence for occasional NG leaks, but they appear  
578 localized and limited in their strength. However, we cannot completely rule out occasional  
579 significant leaks of CH<sub>4</sub> from NG at Indianapolis due to the nature of our assumptions.

580 Overall, assessment of the CH<sub>4</sub> emissions at Indianapolis highlights a number of  
581 uncertainties that need to be considered in any serious evaluation of urban CH<sub>4</sub> emissions. These  
582 uncertainties amplify for Indianapolis since the enhancement signal from its CH<sub>4</sub> emissions is  
583 comparable in magnitude to variability in the regional background flow and as our results show  
584 it may be difficult at times to distinguish noise in the background from the actual city emissions  
585 signal. The evaluation of larger CH<sub>4</sub> sources may be easier with respect to separating signal  
586 from background. However, all of the points raised in this work will be nonetheless relevant and  
587 need to be addressed for our understanding of urban CH<sub>4</sub> emissions to significantly improve.

588

### 589 **Author Contribution**

590 Nikolay Balashov, Kenneth Davis, and Natasha Miles developed the study and worked together  
591 on generating the main hypothesis of this work. They also wrote most of the manuscript.  
592 Nikolay Balashov wrote all of the codes and performed the analyses presented in this work as  
593 well as generated all of the figures. Natasha Miles and Scott Richardson helped with  
594 maintenance and gathering of the INFLUX tower data. They also wrote section 2.2 of the paper.  
595 Thomas Lauvaux helped with the analysis presented in Fig. 1 and section 3.1 concerning  
596 interpretation of the inversion modeling results from Lamb et al. (2016). Thomas Lauvaux also  
597 helped with repeating the inversion experiment for two different Indianapolis domains (Fig. 1).

598 Zachary Barkley significantly contributed to discussions regarding the hypothesis and careful  
599 presentation of sections 2.6 and 3.3. Timothy Bonin provided all of the lidar data and wrote the  
600 second part of section 2.3 regarding the lidar and the methodology used to determine planetary  
601 boundary layer heights. He also contributed to sections 2.6 and 3.3.

602

### 603 **Competing Interests**

604 The authors declare that they have no conflict of interest.

605

### 606 **Acknowledgements**

607 This research has been supported by the National Institute of Standards and Technology (project  
608 number 70NANB10H245). We would like to thank Dr. Bram Maasackers for the helpful  
609 discussion regarding the EPA 2012 inventory and the relevant error structure. We also thank Dr.  
610 Paul Shepson and Dr. Brian Lamb for their useful input regarding airborne mass balance flights  
611 and the process of compiling an emissions inventory. Most importantly, we would like to  
612 acknowledge significant contributions of both reviewers who rigorously examined our science  
613 and noticeably improved clarity of our article.

614

615

### 616 **References**

617

618 Alvarez, R. A., Zavala-Araiza, D., Lyon, D. R., Allen, D. T., Barkley, Z. R., Brandt, A. R.,  
619 Davis, K. J., Herndon, S. C., Jacob, D. J., Karion, A., Kort, E. A., Lamb, B. K., Lauvaux,  
620 T., Maasackers, J. D., Marchese, A. J., Omara, M., Pacala, S. W., Peischl, J., Robinson,  
621 A. L., Shepson, P. B., Sweeney, C., Townsend-Small, A., Wofsy, S. C., and Hamburg, S.  
622 P.: Assessment of methane emissions from the U.S. oil and gas supply chain, *Science*,  
623 10.1126/science.aar7204, 2018.

624 Arya, S. P.: Air pollution meteorology and dispersion, Oxford University Press New York, 1999.

625 Barkley, Z. R., Lauvaux, T., Davis, K. J., Deng, A., Miles, N. L., Richardson, S. J., Cao, Y.,  
626 Sweeney, C., Karion, A., Smith, M., Kort, E. A., Schwietzke, S., Murphy, T., Cervone,  
627 G., Martins, D., and Maasakkers, J. D.: Quantifying methane emissions from natural gas  
628 production in north-eastern Pennsylvania, *Atmos. Chem. Phys.*, 17, 13941-13966,  
629 10.5194/acp-17-13941-2017, 2017.

630 Bakwin, P. S., Tans, P. P., Hurst, D. F., and Zhao, C.: Measurements of carbon dioxide on very  
631 tall towers: results of the NOAA/CMDL program, *Tellus*, 50B, 401–415, 1998.

632 Bonin, T. A., Carroll, B. J., Hardesty, R. M., Brewer, W. A., Hajny, K., Salmon, O. E., and  
633 Shepson, P. B.: Doppler lidar observations of the mixing height in Indianapolis using an  
634 automated composite fuzzy logic approach, *Journal of Atmospheric and Oceanic*  
635 *Technology*, 35, 473-490, 10.1175/jtech-d-17-0159.1, 2018.

636 Brandt, A. R., Heath, G. A., Kort, E. A., O'Sullivan, F., Pétron, G., Jordaan, S. M., Tans, P.,  
637 Wilcox, J., Gopstein, A. M., Arent, D., Wofsy, S., Brown, N. J., Bradley, R., Stucky, G.  
638 D., Eardley, D., and Harriss, R.: Methane leaks from North American natural gas  
639 systems, *Science*, 343, 733-735, 10.1126/science.1247045, 2014.

640 Cambaliza, M., Shepson, P., Bogner, J., Caulton, D., Stirm, B., Sweeney, C., Montzka, S.,  
641 Gurney, K., Spokas, K., and Salmon, O.: Quantification and source apportionment of the  
642 methane emission flux from the city of Indianapolis, *Elem. Sci. Anth.*, 3, 2015.

643 Cambaliza, M. O. L., Shepson, P. B., Caulton, D. R., Stirm, B., Samarov, D., Gurney, K. R.,  
644 Turnbull, J., Davis, K. J., Possolo, A., Karion, A., Sweeney, C., Moser, B., Hendricks, A.,  
645 Lauvaux, T., Mays, K., Whetstone, J., Huang, J., Razlivanov, I., Miles, N. L., and  
646 Richardson, S. J.: Assessment of uncertainties of an aircraft-based mass balance approach  
647 for quantifying urban greenhouse gas emissions, *Atmos. Chem. Phys.*, 14, 9029-9050,  
648 10.5194/acp-14-9029-2014, 2014.

649 Carslaw, D. C., and Ropkins, K.: openair — An R package for air quality data analysis,  
650 *Environmental Modelling & Software*, 27-28, 52-61,  
651 <https://doi.org/10.1016/j.envsoft.2011.09.008>, 2012.

652 Carslaw, D. C., and Bevers, S. D.: Characterising and understanding emission sources using  
653 bivariate polar plots and k-means clustering, *Environmental Modelling & Software*, 40,  
654 325-329, <https://doi.org/10.1016/j.envsoft.2012.09.005>, 2013.



655 Ciais, P., Sabine, C., Bala, G., Bopp, L., Brovkin, V., Canadell, J., Chhabra, A., DeFries, R.,  
656 Galloway, J., and Heimann, M.: Carbon and other biogeochemical cycles, in: Working  
657 Group I Contribution To The IPCC Fifth Assessment Report. Climate Change 2013 - The  
658 Physical Science Basis, edited by: Stocker, T. F., Qin, D., Plattner, G., Tignor, M., Allen,  
659 S., Boschung, J., Nauels, A., Xia, Y., Bex, V., and Midgley, P., Cambridge Univ. Press,  
660 465-570, 2013.

661 Davis, K. J., Deng, A., Lauvaux, T., Miles, N. L., Richardson, S. J., Sarmiento, D. P., Gurney, K.  
662 R., Hardesty, R. M., Bonin, T. A., and Brewer, W. A.: The Indianapolis Flux Experiment  
663 (INFLUX): A test-bed for developing urban greenhouse gas emission measurements,  
664 Elem. Sci. Anth., 5, 2017.

665 Deng, A., Lauvaux, T., Davis, K. J., Gaudet, B. J., Miles, N., Richardson, S. J., Wu, K.,  
666 Sarmiento, D. P., Hardesty, R. M., and Bonin, T. A.: Toward reduced transport errors in a  
667 high resolution urban CO<sub>2</sub> inversion system, Elem. Sci. Anth., 5, 2017.

668 Efron, B., and Tibshirani, R.: Bootstrap methods for standard errors, confidence intervals, and  
669 other measures of statistical accuracy, Statist. Sci., 1, 54-75, 10.1214/ss/1177013815,  
670 1986.

671 European Commission Joint Research Centre, Netherlands Environmental Assessment Agency:  
672 Emission Database for Global Atmospheric Research (EDGAR), Release Version 4.2,  
673 available at: <http://edgar.jrc.ec.europa.eu>, 2010.

674 Gurney, K. R., Razlivanov, I., Song, Y., Zhou, Y., Benes, B., and Abdul-Massih, M.:  
675 Quantification of fossil fuel CO<sub>2</sub> emissions on the building/street scale for a large U.S.  
676 city, Environmental Science & Technology, 46, 12194-12202, 10.1021/es3011282, 2012.

677 Hanna, S. R., Briggs, G. A., and Hosker Jr, R. P.: Handbook on atmospheric diffusion, National  
678 Oceanic and Atmospheric Administration, Oak Ridge, TN (USA). Atmospheric  
679 Turbulence and Diffusion Lab., 1982.

680 Heimbürger, A. M., Harvey, R. M., Shepson, P. B., Stirn, B. H., Gore, C., Turnbull, J.,  
681 Cambaliza, M. O., Salmon, O. E., Kerlo, A.-E. M., and Lavoie, T. N.: Assessing the  
682 optimized precision of the aircraft mass balance method for measurement of urban  
683 greenhouse gas emission rates through averaging, Elem. Sci. Anth., 5, 2017.

684 Helfter, C., Tremper, A. H., Halios, C. H., Kotthaus, S., Björkegren, A., Grimmond, C. S. B.,  
685 Barlow, J. F., and Nemitz, E.: Spatial and temporal variability of urban fluxes of

686 methane, carbon monoxide and carbon dioxide above London, UK, *Atmos. Chem. Phys.*,  
687 16, 10543-10557, 10.5194/acp-16-10543-2016, 2016.

688 Hendrick, M. F., Ackley, R., Sanaie-Movahed, B., Tang, X., and Phillips, N. G.: Fugitive  
689 methane emissions from leak-prone natural gas distribution infrastructure in urban  
690 environments, *Environmental Pollution*, 213, 710-716,  
691 <https://doi.org/10.1016/j.envpol.2016.01.094>, 2016.

692 Hiller, R. V., Neining, B., Brunner, D., Gerbig, C., Bretscher, D., Künzle, T., Buchmann, N.,  
693 and Eugster, W.: Aircraft-based CH<sub>4</sub> flux estimates for validation of emissions from an  
694 agriculturally dominated area in Switzerland, *Journal of Geophysical Research:  
695 Atmospheres*, 119, 4874-4887, doi:10.1002/2013JD020918, 2014.

696 Jackson, R. B., Down, A., Phillips, N. G., Ackley, R. C., Cook, C.W., Plata, D. L., and Zhao, K.  
697 G.: Natural gas pipeline leaks across Washington, DC, *Environ. Sci. Technol.*, 48, 2051–  
698 2058, doi:10.1021/es404474x, 2014.

699 Jeong, S., Millstein, D., and Fischer, M. L.: Spatially explicit methane emissions from petroleum  
700 production and the natural gas system in California, *Environmental Science &  
701 Technology*, 48, 5982-5990, 10.1021/es4046692, 2014.

702 Jeong, S., Newman, S., Zhang, J., Andrews, A. E., Bianco, L., Bagley, J., Cui, X., Graven, H.,  
703 Kim, J., Salameh, P., LaFranchi, B. W., Priest, C., Campos-Pineda, M., Novakovskaia,  
704 E., Sloop, C. D., Michelsen, H. A., Bambha, R. P., Weiss, R. F., Keeling, R., and Fischer,  
705 M. L.: Estimating methane emissions in California's urban and rural regions using  
706 multitower observations, *Journal of Geophysical Research: Atmospheres*, 121, 13,031-  
707 013,049, doi:10.1002/2016JD025404, 2016.

708 Jeong, S., Cui, X., Blake, D. R., Miller, B., Montzka, S. A., Andrews, A., Guha, A., Martien, P.,  
709 Bambha, R. P., LaFranchi, B., Michelsen, H. A., Clements, C. B., Glaize, P., and Fischer,  
710 M. L.: Estimating methane emissions from biological and fossil-fuel sources in the San  
711 Francisco Bay Area, *Geophysical Research Letters*, 44, 486-495,  
712 doi:10.1002/2016GL071794, 2017.

713 Karion, A., Sweeney, C., Kort, E. A., Shepson, P. B., Brewer, A., Cambaliza, M., Conley, S. A.,  
714 Davis, K., Deng, A., Hardesty, M., Herndon, S. C., Lauvaux, T., Lavoie, T., Lyon, D.,  
715 Newberger, T., Pétron, G., Rella, C., Smith, M., Wolter, S., Yacovitch, T. I., and Tans,

716 P.: Aircraft-based estimate of total methane emissions from the Barnett Shale region,  
717 Environ. Sci. Technol., 49, 8124–8131, doi:10.1021/acs.est.5b00217, 2015

718 Kort, E. A., Eluszkiewicz, J., Stephens, B. B., Miller, J. B., Gerbig, C., Nehrkorn, T., Daube, B.  
719 C., Kaplan, J. O., Houweling, S., and Wofsy, S. C.: Emissions of CH<sub>4</sub> and N<sub>2</sub>O over the  
720 United States and Canada based on a receptor-oriented modeling framework and  
721 COBRA-NA atmospheric observations, Geophys. Res. Lett., 35, L18808,  
722 doi:10.1029/2008GL034031, 2008.

723 Lamb, B. K., Cambaliza, M. O. L., Davis, K. J., Edburg, S. L., Ferrara, T. W., Floerchinger, C.,  
724 Heimburger, A. M. F., Herndon, S., Lauvaux, T., Lavoie, T., Lyon, D. R., Miles, N.,  
725 Prasad, K. R., Richardson, S., Roscioli, J. R., Salmon, O. E., Shepson, P. B., Stirm, B. H.,  
726 and Whetstone, J.: Direct and indirect measurements and modeling of methane emissions  
727 in Indianapolis, Indiana, Environmental Science & Technology, 50, 8910-8917,  
728 10.1021/acs.est.6b01198, 2016.

729 Lauvaux, T., Miles, N. L., Deng, A., Richardson, S. J., Cambaliza, M. O., Davis, K. J., Gaudet,  
730 B., Gurney, K. R., Huang, J., O'Keefe, D., Song, Y., Karion, A., Oda, T., Patarasuk, R.,  
731 Razlivanov, I., Sarmiento, D., Shepson, P., Sweeney, C., Turnbull, J., and Wu, K.: High-  
732 resolution atmospheric inversion of urban CO<sub>2</sub> emissions during the dormant season of  
733 the Indianapolis Flux Experiment (INFLUX), Journal of Geophysical Research:  
734 Atmospheres, 121, 5213-5236, doi:10.1002/2015JD024473, 2016.

735 Maasackers, J. D., Jacob, D. J., Sulprizio, M. P., Turner, A. J., Weitz, M., Wirth, T., Hight, C.,  
736 DeFigueiredo, M., Desai, M., Schmeltz, R., Hockstad, L., Bloom, A. A., Bowman, K.  
737 W., Jeong, S., and Fischer, M. L.: Gridded national inventory of U.S. methane emissions,  
738 Environmental Science & Technology, 50, 13123-13133, 10.1021/acs.est.6b02878, 2016.

739 Mays, K. L., Shepson, P. B., Stirm, B. H., Karion, A., Sweeney, C., and Gurney, K. R.: Aircraft-  
740 based measurements of the carbon footprint of Indianapolis, Environmental Science &  
741 Technology, 43, 7816-7823, 10.1021/es901326b, 2009.

742 McKain, K., Down, A., Raciti, S. M., Budney, J., Hutyrá, L. R., Floerchinger, C., Herndon, S.  
743 C., Nehrkorn, T., Zahniser, M. S., Jackson, R. B., Phillips, N., and Wofsy, S. C.: Methane  
744 emissions from natural gas infrastructure and use in the urban region of Boston,  
745 Massachusetts, Proceedings of the National Academy of Sciences, 112, 1941-1946,  
746 10.1073/pnas.1416261112, 2015.

747 Miles, N. L., Richardson, S. J., Lauvaux, T., Davis, K. J., Balashov, N. V., Deng, A., Turnbull, J.  
748 C., Sweeney, C., Gurney, K. R., and Patarasuk, R.: Quantification of urban atmospheric  
749 boundary layer greenhouse gas dry mole fraction enhancements in the dormant season:  
750 Results from the Indianapolis Flux Experiment (INFLUX), *Elem. Sci. Anth.*, 5, 2017.

751 Miller, S. M., Wofsy, S. C., Michalak, A. M., Kort, E. A., Andrews, A. E., Biraud, S. C.,  
752 Dlugokencky, E. J., Eluszkiewicz, J., Fischer, M. L., Janssens-Maenhout, G., Miller, B.  
753 R., Miller, J. B., Montzka, S. A., Nehrkorn, T., and Sweeney, C.: Anthropogenic  
754 emissions of methane in the United States, *Proceedings of the National Academy of*  
755 *Sciences*, 110, 20018-20022, 10.1073/pnas.1314392110, 2013.

756 Myhre, G., Shindell, D., Bréon, F. M., Collins, W., Fuglestvedt, J., Huang, J., Koch, D.,  
757 Lamarque, J. F., Lee, D., Mendoza, B., Nakajima, T., Robock, A., Stephens, G.,  
758 Takemura, T., and Zhang, H.: Anthropogenic and natural radiative forcing, in: *Climate*  
759 *Change 2013: The Physical Science Basis. Contribution of Working Group I to the Fifth*  
760 *Assessment Report of the Intergovernmental Panel on Climate Change*, edited by:  
761 Stocker, T. F., Qin, D., Plattner, G. K., Tignor, M., Allen, S. K., Doschung, J., Nauels,  
762 A., Xia, Y., Bex, V., and Midgley, P. M., Cambridge University Press, Cambridge, UK,  
763 659-740, 2013.

764 National Academies of Sciences and Medicine: Improving characterization of anthropogenic  
765 methane emissions in the United States, The National Academies Press, Washington, DC,  
766 250 pp., 2018.

767 Nisbet, E. G., Dlugokencky, E. J., Manning, M. R., Lowry, D., Fisher, R. E., France, J. L.,  
768 Michel, S. E., Miller, J. B., White, J. W. C., Vaughn, B., Bousquet, P., Pyle, J. A.,  
769 Warwick, N. J., Cain, M., Brownlow, R., Zazzeri, G., Lanoisellé, M., Manning, A. C.,  
770 Gloor, E., Worthy, D. E. J., Brunke, E.-G., Labuschagne, C., Wolff, E. W., and Ganesan,  
771 A. L.: Rising atmospheric methane: 2007–2014 growth and isotopic shift, *Global*  
772 *Biogeochemical Cycles*, 30, 1356-1370, doi:10.1002/2016GB005406, 2016.

773 Richardson, S. J., Miles, N. L., Davis, K. J., Lauvaux, T., Martins, D. K., Turnbull, J. C.,  
774 McKain, K., Sweeney, C., and Cambaliza, M. O. L.: Tower measurement network of in-  
775 situ CO<sub>2</sub>, CH<sub>4</sub>, and CO in support of the Indianapolis FLUX (INFLUX) Experiment,  
776 *Elem Sci Anth*, 5, 2017.

777 Sarmiento, D. P., Davis, K. J., Deng, A., Lauvaux, T., Brewer, A., and Hardesty, M.: A  
778 comprehensive assessment of land surface-atmosphere interactions in a WRF/Urban  
779 modeling system for Indianapolis, IN, *Elem. Sci. Anth.*, 5, 2017.

780 Saunio, M., Jackson, R. B., Bousquet, P., Poulter, B., and Canadell, J. G.: The growing role of  
781 methane in anthropogenic climate change, *Environmental Research Letters*, 11, 120207,  
782 2016.

783 Schuh, A. E., Lauvaux, T., West, T. O., Denning, A. S., Davis, K. J., Miles, N., Richardson, S.,  
784 Uliasz, M., Lokupitiya, E., Cooley, D., Andrews, A., and Ogle, S.: Evaluating  
785 atmospheric CO<sub>2</sub> inversions at multiple scales over a highly inventoried agricultural  
786 landscape, *Global change biology*, 19, 1424-1439, doi:10.1111/gcb.12141, 2013.

787 Taylor, D. M., Chow, F. K., Delkash, M., and Imhoff, P. T.: Atmospheric modeling to assess  
788 wind dependence in tracer dilution method measurements of landfill methane emissions,  
789 *Waste Management*, 73, 197-209, <https://doi.org/10.1016/j.wasman.2017.10.036>, 2018.

790 Townsend-Small, A., Tyler, S. C., Pataki, D. E., Xu, X., and Christensen, L. E.: Isotopic  
791 measurements of atmospheric methane in Los Angeles, California, USA: Influence of  
792 “fugitive” fossil fuel emissions, *J. Geophys. Res.-Atmos.*, 117, 1–11,  
793 <https://doi.org/10.1029/2011JD016826>, 2012.

794 Turnbull, J. C., Sweeney, C., Karion, A., Newberger, T., Lehman, S. J., Tans, P. P., Davis, K. J.,  
795 Lauvaux, T., Miles, N. L., Richardson, S. J., Cambaliza, M. O., Shepson, P. B., Gurney,  
796 K., Patarasuk, R., and Razlivanov, I.: Toward quantification and source sector  
797 identification of fossil fuel CO<sub>2</sub> emissions from an urban area: Results from the INFLUX  
798 experiment, *Journal of Geophysical Research: Atmospheres*, 120, 292-312,  
799 doi:10.1002/2014JD022555, 2015.

800 Turnbull, J. C., Karion, A., Davis, K. J., Lauvaux, T., Miles, N. L., Richardson, S. J., Sweeney,  
801 C., McKain K., Lehman, S. J., Gurney, K., Patarasuk, R., Jianming L., Shepson, P. B.,  
802 Heimbürger A., Harvey, R., and Whetstone, J.: Synthesis of urban CO<sub>2</sub> emission  
803 estimates from multiple methods from the Indianapolis Flux Project (INFLUX),  
804 *Environmental Science and Technology*, 53 (1), 287-295, 10.1021/acs.est.8b05552, 2019.

805 U.S. Environmental Protection Agency: Inventory of U.S. Greenhouse Gas Emissions and Sinks:  
806 1990–2011, Technical Report EPA 430-R-13-001, Environmental Protection Agency,  
807 Washington, 505 pp., 2013.

808 Van De Wiel, B. J. H. V. d., Moene, A. F., Jonker, H. J. J., Baas, P., Basu, S., Donda, J. M. M.,  
809 Sun, J., and Holtslag, A. A. M.: The minimum wind speed for sustainable turbulence in  
810 the nocturnal boundary layer, *Journal of the Atmospheric Sciences*, 69, 3116-3127,  
811 10.1175/jas-d-12-0107.1, 2012.

812 Wunch, D., Wennberg, P. O., Toon, G. C., Keppel-Aleks, G., and Yavin, Y. G.: Emissions of  
813 greenhouse gases from a North American megacity, *Geophysical Research Letters*, 36,  
814 doi:10.1029/2009GL039825, 2009.

815 Zavala-Araiza, D., Lyon, D. R., Alvarez, R. A., Davis, K. J., Harriss, R., Herndon, S. C., Karion,  
816 A., Kort, E. A., Lamb, B. K., Lan, X., Marchese, A. J., Pacala, S. W., Robinson, A. L.,  
817 Shepson, P. B., Sweeney, C., Talbot, R., Townsend-Small, A., Yacovitch, T. I.,  
818 Zimmerle, D. J., and Hamburg, S. P.: Reconciling divergent estimates of oil and gas  
819 methane emissions, *Proceedings of the National Academy of Sciences*, 112, 15597-  
820 15602, 10.1073/pnas.1522126112, 2015.

821  
822  
823  
824  
825  
826  
827  
828  
829  
830  
831  
832  
833  
834  
835  
836  
837  
838  
839  
840  
841  
842  
843  
844  
845  
846  
847

848  
 849  
 850  
 851  
 852  
 853  
 854  
 855  
 856  
 857  
 858  
 859  
 860  
 861  
 862  
 863  
 864  
 865  
 866  
 867  
 868  
 869  
 870

**Tables**

**Table 1.** INFLUX towers used to estimate CH<sub>4</sub> background based on two different criteria. Numbers in bold indicate towers chosen to generate a background field when multiple options are possible (for more details see discussion). In short, criterion 1 uses towers with the lowest mean CH<sub>4</sub> for a specific wind direction, and criterion 2 uses towers outside of Marion County and not downwind of large sources (including the city as a whole).

Wind Direction	CH <sub>4</sub> Background Towers	
	Criterion 1	Criterion 2
North (N)	8	<b>13</b> , 8
Northeast (NE)	8	<b>13</b> , 8, 2
East (E)	<b>2</b> , 8	<b>8</b> , 4, 1, 2
Southeast (SE)	1	<b>8</b> , 13, 4, 1
South (S)	1	<b>4</b> , 13, 1
Southwest (SW)	13	<b>1</b> , 4
West (W)	1	<b>4</b> , 1
Northwest (NW)	1	<b>8</b> , 1

871  
 872  
 873

874  
875  
876  
877  
878  
879  
880  
881  
882  
883  
884  
885  
886  
887  
888 **Table 2.** A number of independent samples needed (column 4) to satisfy combined requirement of 6 ppb  
889 background error based on the sum of bias and random error (explained in section 3.2) as a function of  
890 wind direction.

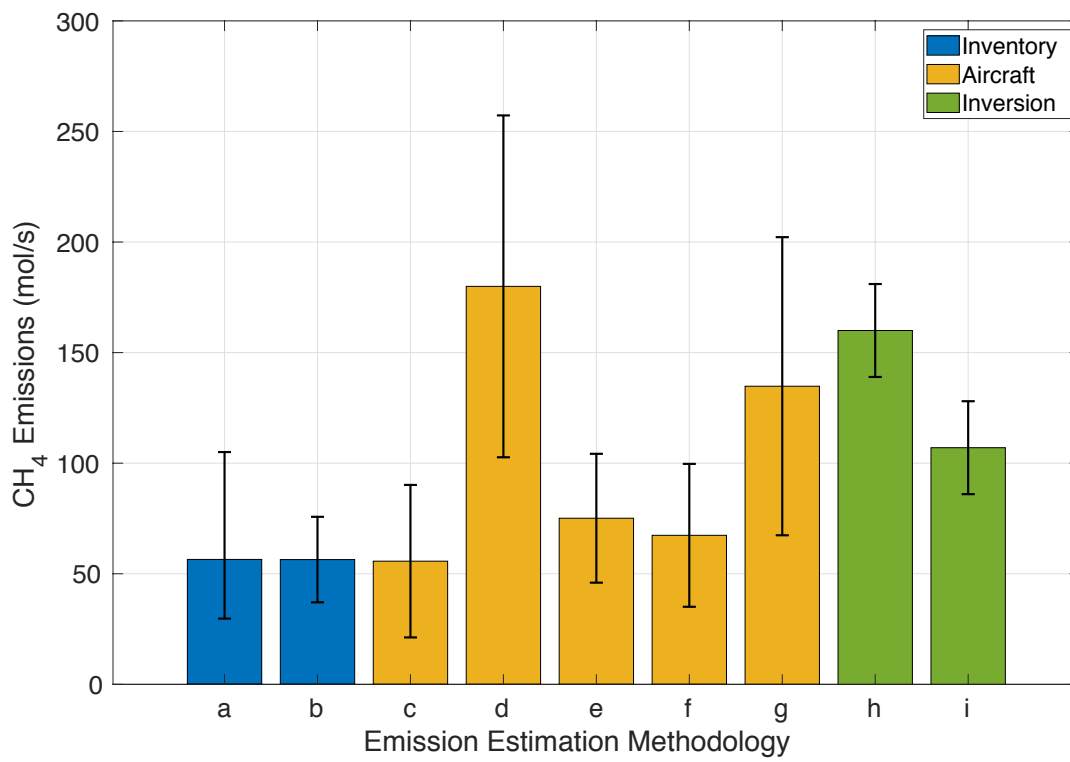
Wind Direction	Bias (ppb)	Threshold (ppb)	Samples Needed
N	1	5	74
NE	1	5	36
E	0.5	5.5	46
SE	4	2	>150
S	2	4	53
SW	4.5	1.5	>150
W	3	3	52
NW	5	1	>150

891  
892  
893  
894  
895  
896  
897  
898  
899  
900  
901  
902  
903



904  
905  
906  
907  
908  
909  
910  
911  
912  
913  
914  
915  
916  
917  
918  
919  
920  
921  
922  
923  
924

**Figures**

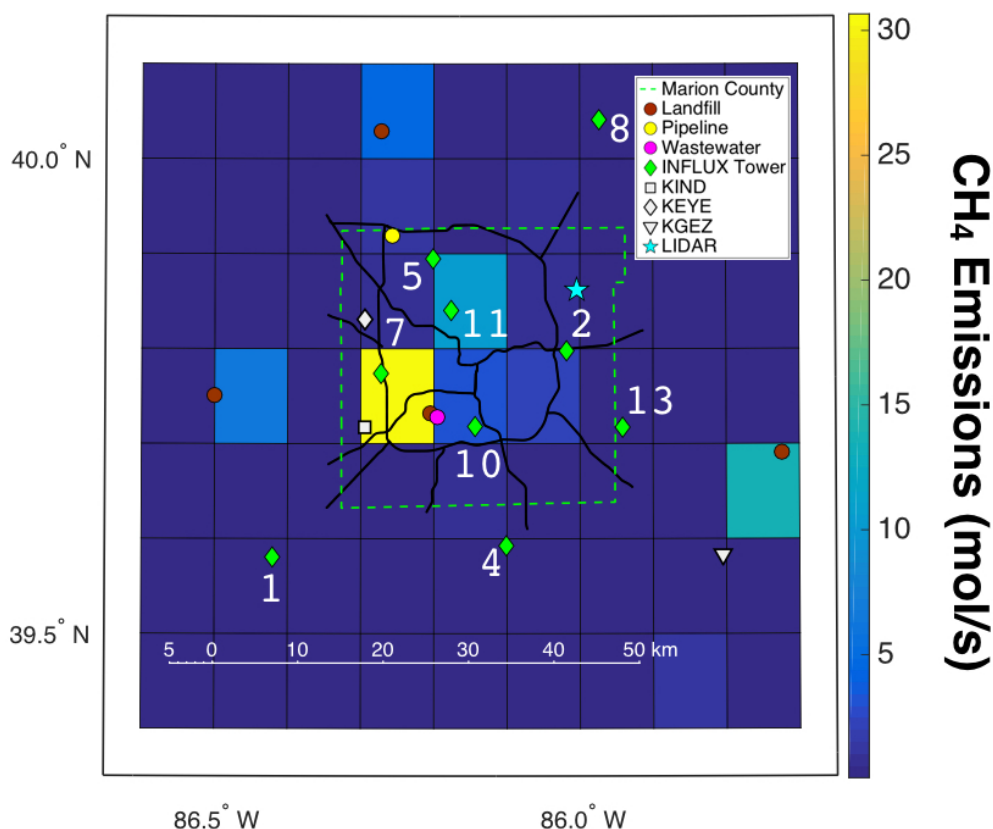


925

926 **Figure 1.** Various estimates of CH<sub>4</sub> emissions at Indianapolis. (a, b) Bottom-up estimates of CH<sub>4</sub>  
927 emissions conducted by Lamb et al. (2016) in 2013 and Maasackers et al. (2016) based on the EPA 2012

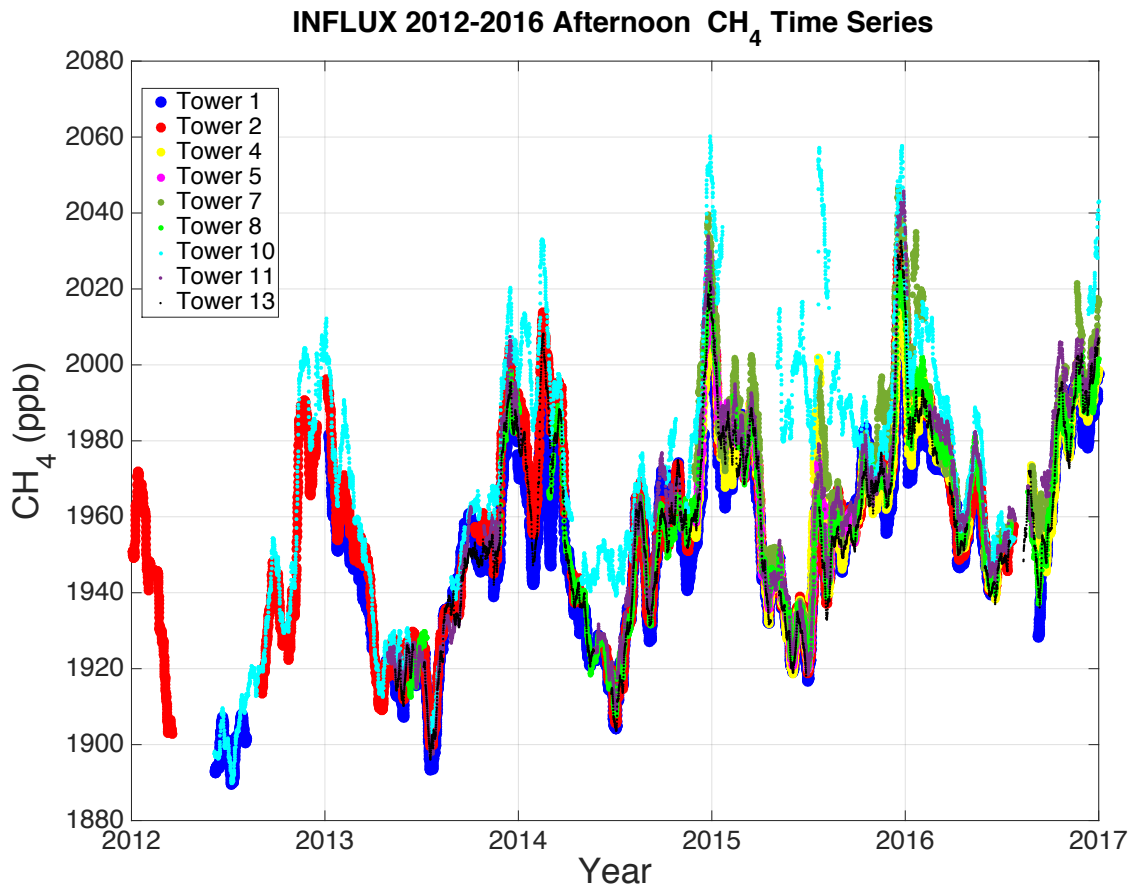
928 inventory respectively. Error bars show 95% confidence intervals (for more details see above-mentioned  
 929 articles). **(c-g)** Top-down evaluations of CH<sub>4</sub> emissions with aircraft from various flight campaigns where  
 930 **(c)** contains 5 flights over March-April of 2008, **(d)** contains 3 flights over November-January of 2008-  
 931 09, **(e)** contains 5 flights over April-July of 2011, **(f)** contains 9 flights from November-December, 2014,  
 932 and **(g)** contains the same 5 flights over April-July of 2011 as in (e) but uses different methodology.  
 933 Methodologies for **(c-f)** are described in Lamb et al. (2016) and methodology for **(g)** is described in  
 934 Cambaliza et al. (2015). Error bars show 95% confidence intervals (for more details see above-  
 935 mentioned articles). **(h, i)** Top-down evaluations of CH<sub>4</sub> emissions for 2012-2013 using tower inversion  
 936 modeling methodology with two different domains, where **(h)** uses the full domain of Figure 2 and **(i)**  
 937 uses only the Marion County domain of Figure 2. The inversion methodology and 95% confidence  
 938 intervals are described in detail in Lamb et al. (2016).

939  
 940  
 941  
 942



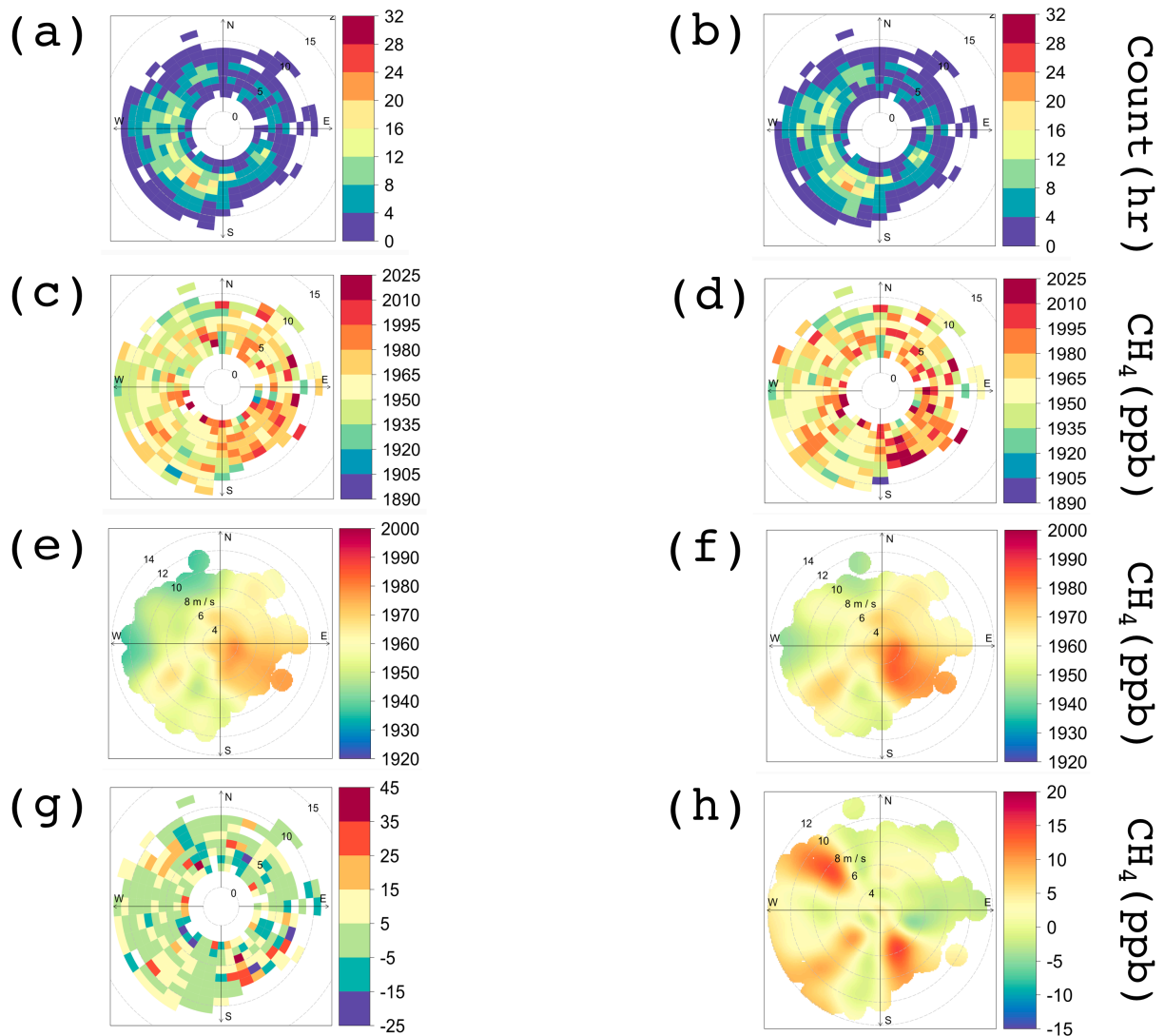
943  
 944 **Figure 2.** Map of the primary roads in Indianapolis, INFLUX towers, lidar system, weather stations, and  
 945 a few CH<sub>4</sub> point sources plotted over the gridded CH<sub>4</sub> emissions (mol/s) from the EPA 2012 Inventory  
 946 (Maasakkers et al., 2016). The gridded map of emissions includes emissions from the mentioned point  
 947 sources; their position is provided to aid in interpretation of the observations. The dashed bright green  
 948 line denotes Marion County borders.

949



950

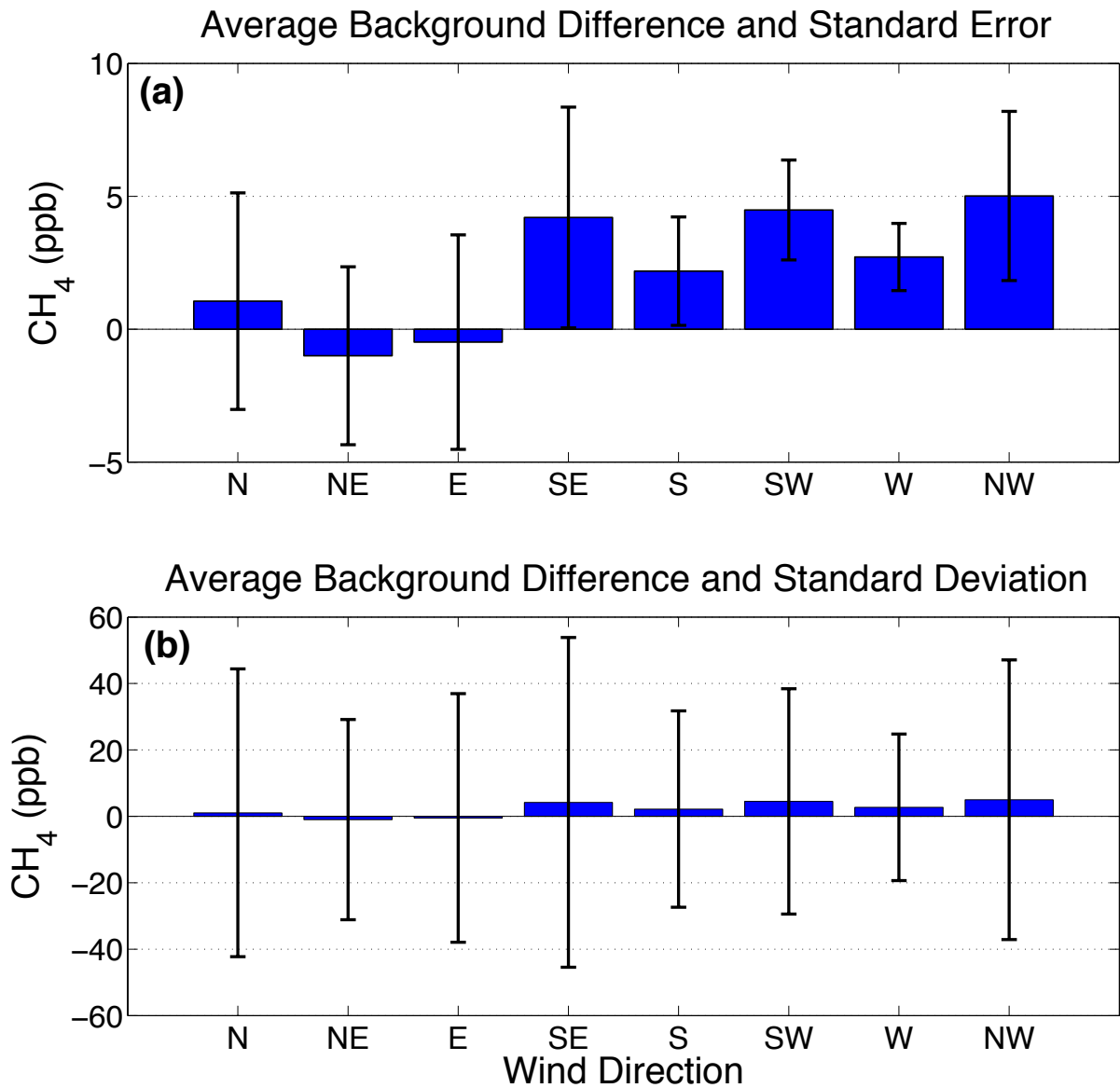
951 **Figure 3.** 20-day running average of afternoon (12-16 LST; the hours are inclusive) CH<sub>4</sub> mole fractions  
952 as measured by the INFLUX tower network (highest available height is used) from 2012 through 2016.



953

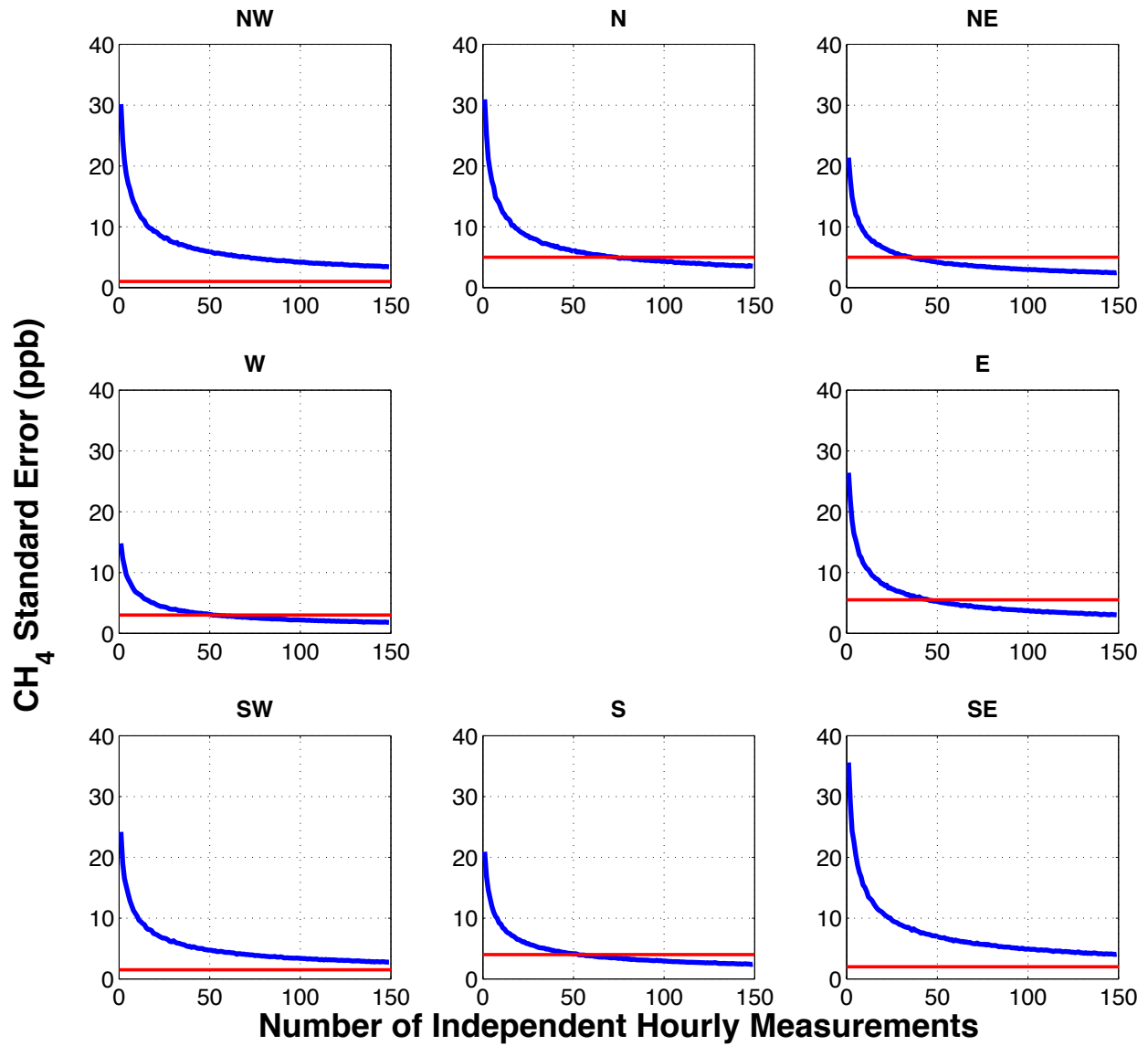
954 **Figure 4.** Frequency and bivariate polar plots of CH<sub>4</sub> background for Indianapolis using data from 12-16  
 955 LST, November 2014 through December 2016 given 2 different criteria (Table 1). **(a)** Polar histogram  
 956 indicating a number of hourly measurements available using criterion 1. **(b)** Same as (a) only for criterion  
 957 2. Differences between (a) and (b) are due to slight differences in data availability at the considered  
 958 towers. **(c)** Polar frequency plot of the CH<sub>4</sub> background using criterion 1. **(d)** Same as (c) only for  
 959 criterion 2. **(e)** Polar bivariate plot of CH<sub>4</sub> background using criterion 1. **(f)** Same as (e) only for  
 960 criterion 2. **(g)** Polar frequency plot of difference between the backgrounds: *criterion 2 – criterion 1*. **(h)** Same  
 961 as (g) but shown with a bivariate polar plot.

962



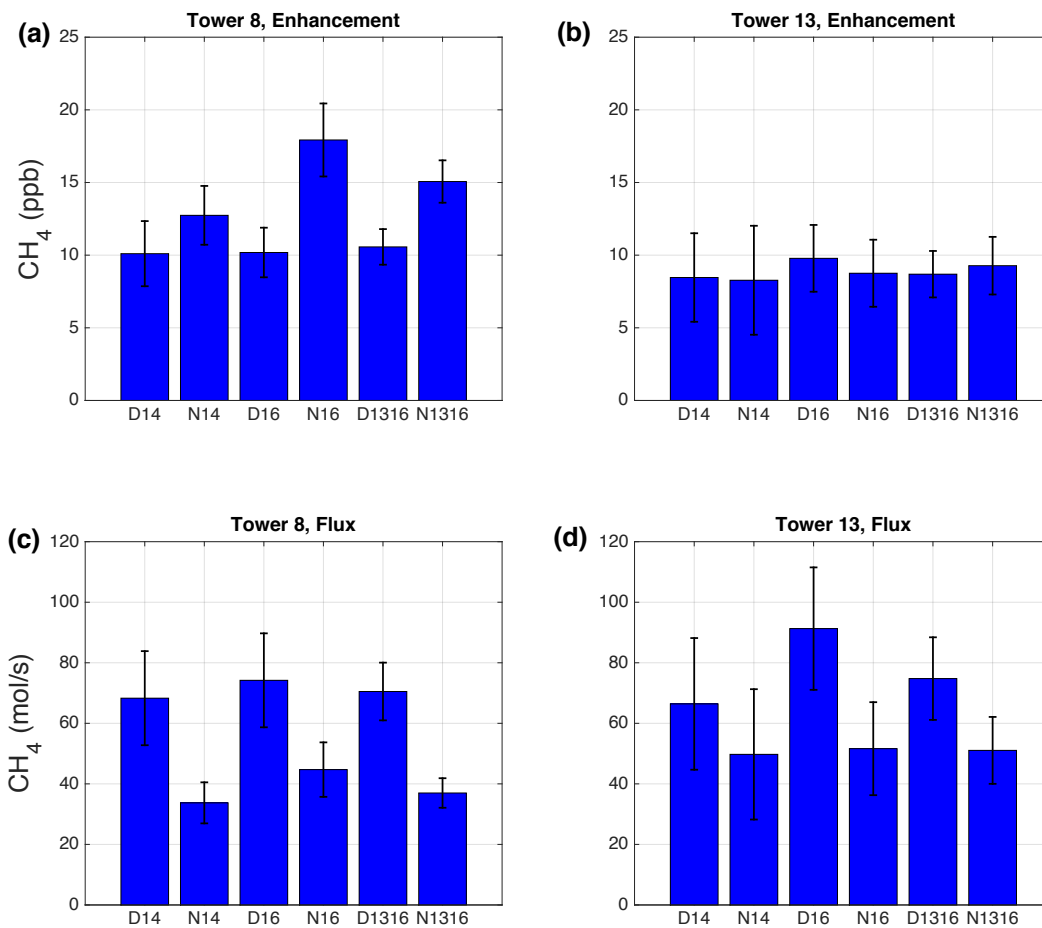
963  
 964 **Figure 5.** Average of the differences between criteria 2 and 1 CH<sub>4</sub> backgrounds at Indianapolis as a  
 965 function of wind direction. These averages are generated from the same data that is used in Figure 4 and  
 966 reflect results shown in Figure 4g. Error bars indicate in (a) 2 × standard error and in (b) 2 × standard  
 967 deviation.

968



969  
 970  
 971  
 972  
 973

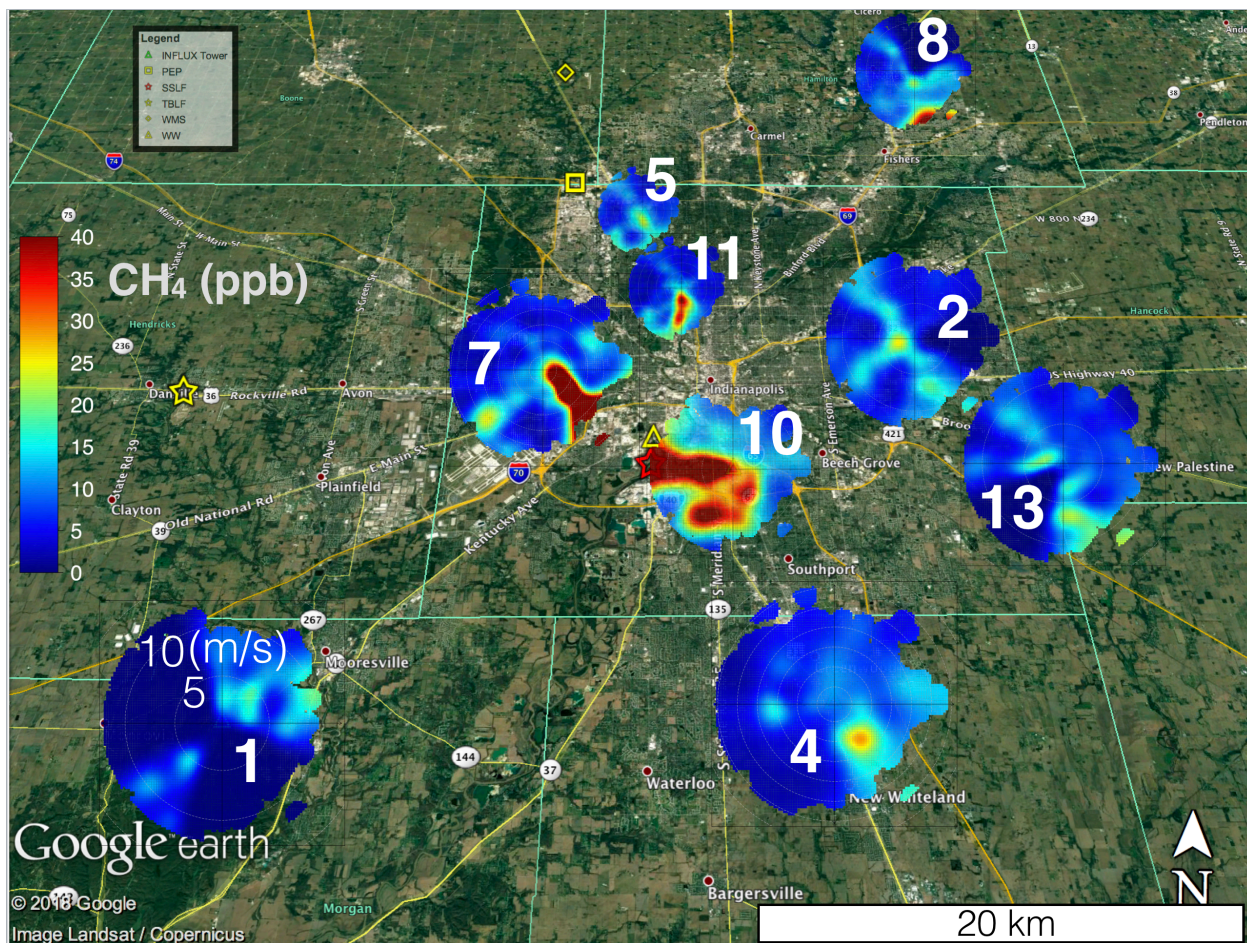
**Figure 6.** Bootstrap simulation of the standard errors  $\times 2$  in Indianapolis CH<sub>4</sub> background mole fraction differences (between criteria 2 and 1) as a function of sample size and wind direction (see text for details). Thresholds for each of the wind directions indicate a random error threshold needed for the background uncertainty to be within 50% of Indianapolis CH<sub>4</sub> enhancement of 12 ppb.



975

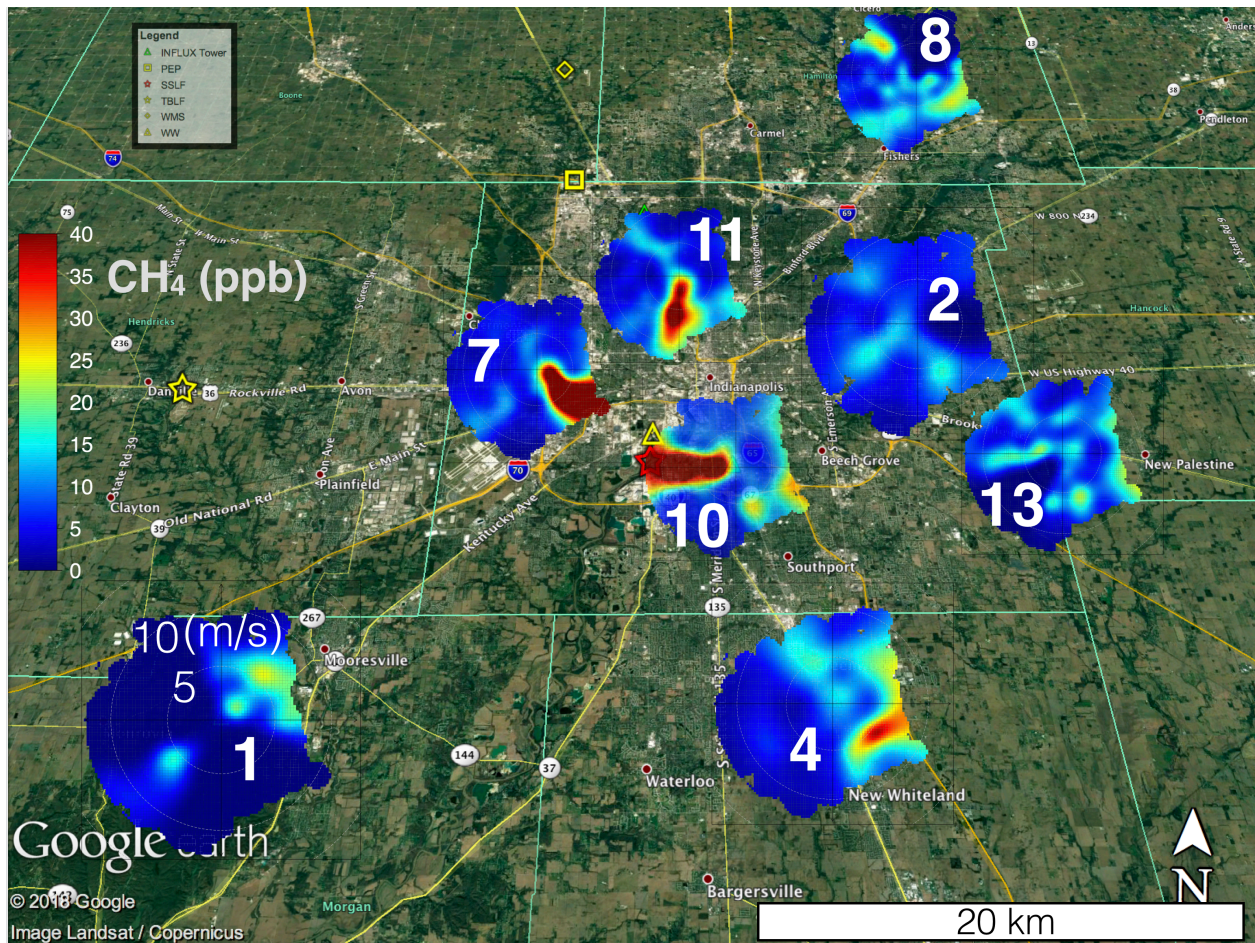
976 **Figure 7.** Averages of the daytime (D) and nighttime (N) CH<sub>4</sub> enhancements and fluxes at INFLUX  
 977 towers 8 and 13 for years 2014 (14), 2016 (16), and 2013-2016 (1316). The error bars represent 95%  
 978 confidence interval of each mean value. **(a)** Estimates of CH<sub>4</sub> enhancements from tower 8. **(b)** Estimates  
 979 of CH<sub>4</sub> enhancements from tower 13. **(c)** Estimates of CH<sub>4</sub> flux from tower 8. **(d)** Estimates of CH<sub>4</sub> flux  
 980 from tower 13.





981  
 982 **Figure 8.** Google Earth image overlaid with bivariate polar plots (section 2.5) of the CH<sub>4</sub> enhancements  
 983 at 9 INFLUX towers in Indianapolis using the criterion 1 background (Table 1) for full years of 2014 and  
 984 2015 over the afternoon (12-16 LST). The wind speed scale is only labeled at site 1; other sites follow  
 985 the same convention. Legend indicates known sources of CH<sub>4</sub>: Panhandle Eastern Pipeline (PEP),  
 986 Southern Side Landfill (SSLF), Twin Bridges Landfill (TBLF), Waste Management Solutions (WMS),  
 987 and Waste Water treatment facility (WW). The known magnitudes of sources that are in Marion County  
 988 (PEP, SSLF, and WW) are reported in section 2.7. Magnitudes of TBLF and WMS according to EPA are  
 989 approximately 5 mol/s. The largest known source on the map is SSLF.





990

991 **Figure 9.** Google Earth image overlaid with bivariate polar plots (section 2.5) of the CH<sub>4</sub> enhancements  
 992 at 9 INFLUX towers in Indianapolis using the criterion 1 background (Table 1) for year 2016 over the  
 993 afternoon (12-16 LST). The wind speed scale is only labeled at site 1; other sites follow the same  
 994 convention. Legend indicates known sources of CH<sub>4</sub>: Panhandle Eastern Pipeline (PEP), Southern Side  
 995 Landfill (SSLF), Twin Bridges Landfill (TBLF), Waste Management Solutions (WMS), and Waste Water  
 996 treatment facility (WW). The known magnitudes of sources that are in Marion County (PEP, SSLF, and  
 997 WW) are reported in section 2.7. Magnitudes of TBLF and WMS according to EPA are approximately 5  
 998 mol/s. The largest known source on the map is SSLF.